2023

Machine-Learning Based Model Predictive Control for a Three-phase Inverter

Arturo De La Cruz
Minnesota State University, Mankato

Recommended Citation

De La Cruz, Arturo. (2023). *Machine-Learning Based Model Predictive Control for a Three-phase Inverter*. [Master’s thesis, Minnesota State University, Mankato]. Cornerstone: A Collection of Scholarly and Creative Works for Minnesota State University, Mankato. https://cornerstone.lib.mnsu.edu/etds/1390/

Machine-Learning Based Model Predictive Control for a Three-phase Inverter.

By

Arturo De La Cruz

A THESIS

Presented to the Faculty of

The Graduate College at Minnesota State University, Mankato

In Partial Fulfillment of Requirements

For the Degree of Master of Science

Major: Electrical Engineering

Under the Supervision of Professor Jianwu Zeng

Mankato, Minnesota

November 2023

11/14/2023

Machine-Learning Based Model Predictive Control for a Three-phase Inverter.

Arturo A. De La Cruz Campos

This thesis has been examined and approved by the following members of the student’s committee.

Advisor

Committee Member

Committee Member

Advisor: Dr. Jianwu Zeng.

In recent years, the study of three-phase inverter controls has become important with the rising use of renewable energy sources (RES) in the form of distribution generation (DG). Many control types have been developed for DG inverters and others were traditional controls for the generation of the main grid power that were adapted for a system with less inertia. Among these controls is the model predictive control (MPC) which allows for a fast transient response and good reference tracking. One disadvantage of the MPC is that it does this prediction and optimization online which can limit the applications due to computational loading. Although there are some solutions to this problem in the form of a finite control-set MPC (FCS-MPC) which takes advantage of the only two states of a switch mode converter to reduce complexity, this still takes the form of a nonlinear online optimization problem.

However, compared with the continuous control set (CCS) MPC, using the FCS-MPC may result in poor performance due to the degradation of the switching frequency. The high computation of CCS-MPC prevents it from being implemented in the resources-limited digital signal processor (DSP). To reduce the computational burden, machine learning (ML) methods such as artificial neural networks (ANN) are used for learning the input and output of the MPC. This thesis compares the ANN-MPC, and support vector machine (SVM) based MPC in a three-phase inverter. A comparison of total harmonic distortion (THD), and reference tracking during different scenarios will be provided.

Table of Contents

Chapter 1 : Introduction 1

1.1 Background 1

1.2. Control Schemes for Power Converters 1

1.2.1 Modelling the System 2

1.2.2 Rotational Reference Frames 3

1.2.3 PID Control 5

1.3 A literature Review of the MPC 6

1.3.1 The Model Predictive Control 6

1.3.2 Cost Function and Optimization 8

1.3.3 Disadvantages 9

Chapter 2 : Literature Review of Machine Learning Based MPC........................ 10

2.1 Machine Learning Based MPC 10

2.1.1 Structure 10

2.1.2 Data Preprocessing.. 15

2.1.3 Training and Fitting Performance. 15

Chapter 3 : Simulations.. 17

3.1 Simulation Studies 17

3.2 Simulation Results 26

3.2.1 Steady-State Linear Load ... 26

3.2.2 Dynamic Loads ... 31

3.2.3 Steady-state Nonlinear Load ... 34

Chapter 4 : Experimental Results ... 40

4.1 Testing overview and set-up ... 40

4.2 Testing Scenarios ... 41

4.2.1 Static Loads ... 41

4.2.2 Dynamic load test ... 53

4.2.3 Nonlinear loading ... 56

4.3 Computational Time Comparison ... 64

Chapter 5 : Conclusions and Recommendations for the Future Research ... 68

References ... 69

List of Publications ... 72

List of Figures

Figure 1.1: Half-bridge voltage-source inverter. 2

Figure 1.2: Three-phase voltages and its Clarke transform representation. 3

Figure 1.3: alpha-beta and DQZ transform...4

Figure 1.4: PID control structure. 5

Figure 1.5: Voltage and current control loops. 6

Figure 1.6 MPC Control loop with a three-step control horizon. 7

Figure 1.7: MPC online optimization in discrete time...8

Figure 2.1: ANN architecture. 11

Figure 2.2: SVM hyperplane..13

Figure 2.3: Epsilon tube..14

Figure 2.4: Overfitting of the SVM. 16

Figure 3.1: MPC design tool...18

Figure 3.2: Inverter and MPC control loop...19

Figure 3.3: MPC performance. 20

Figure 3.4: MPC error tracking...20

Figure 3.5: THD and error versus SVM parameters...21

Figure 3.6: RBFSVM-MPC outputs and reference...22

Figure 3.7: RBF-SVM-MPC error tracking..23

Figure 3.8: RBF-SVM-MPC controller block. 23

Figure 3.9: ANN Simulink model..24

Figure 3.10: ANN training...25

Figure 3.11: ANN training data error. 25

Figure 3.12: THD comparison between the three controls. 27

Figure 3.13: Error tracking at 47 Ohms. 28

Figure 3.14: inverter THD at 32 Ohms load. 29

Figure 3.15: Controls' error at R = 32 Ohms 29

Figure 3.16: Simulated THD performance with a static linear load. 30

Figure 3.17: Simulated tracking error with a resistive load.................................31

Figure 3.18: Dynamic load Simulink set-up. 32

Figure 3.19: MPC performance during a sudden load switch. 32

Figure 3.20: SVM performance during a sudden load switch. 33

Figure 3.21: ANN performance during a sudden load switch. 33

Figure 3.22: Nonlinear load Simulink model. 34

Figure 3.23: MPC performance to nonlinear load. 35

Figure 3.24: SVM performance to nonlinear load. 35

Figure 3.25: ANN performance to nonlinear load. 36

Figure 3.26: Controllers' THD for nonlinear loading..37

Figure 3.27: Controllers' tracking error for nonlinear loading. 37

Figure 3.28: Controllers' tracking error for nonlinear loading. 38

Figure 3.29: Controllers' tracking error for nonlinear loading. 39

Figure 4.1: Three-phase inverter set-up. 41

Figure 4.2: MPC's performance with a 47Ω load...42

Figure 4.3: MPC's error tracking with a 47-ohm load...43

Figure 4.4: ANN controller's performance with a 47ohm load. 44

Figure 4.5: ANN controller’s error tracking with a 47-ohm load.........................45

Figure 4.6: SVM-MPC’s performance at 47-ohm. 46

Figure 4.7: SVM error tracking with 47-ohms. 46

Figure 4.8: MPC’s performance with a 32-ohm load. 47

Figure 4.9: MPC’s error tracking with a 32-ohm load...48

Figure 4.10: ANN-MPC performance with a 32-ohm load. 49

Figure 4.11: ANN control error tracking with a 32-ohm load. 49

Figure 4.12: SVM-MPC performance with a 32-ohm load. 50

Figure 4.13: SVM-MPC error tracking with a 32-ohm load. 51

Figure 4.14 Control THD at different resistive loads. 52

Figure 4.15 Control MAE at different resistive loads..53

Figure 4.16: MPC performance during load change..54

Figure 4.17: ANN-MPC control performance during load change 55

Figure 4.18: SVM-MPC control performance during load change. 56

Figure 4.19: Nonlinear load experimental set-up. 57

Figure 4.20: MPC performance with a nonlinear load. 58

Figure 4.21: MPC error tracking with a nonlinear load.......................................59

Figure 4.22: ANN-MPC control performance with a nonlinear load. 60

Figure 4.23: ANN-MPC reference tracking error with a nonlinear load. 60

Figure 4.24: SVM performance with a nonlinear load. 61

Figure 4.25: SVM performance with a nonlinear load. 62

Figure 4.26: SVM performance with a nonlinear load. 63

Figure 4.27: SVM performance with a nonlinear load. 64

Figure 4.28: Microcontroller CPU loading with MPC. 65

Figure 4.29: Microcontroller CPU loading with ANN. 65

Figure 4.30: Microcontroller CPU loading with SVM. 66

Acknowledgements

I would like to thank Dr. Jianwu Zeng for providing the opportunity to work on this project. His support and knowledge were indispensable for me when completing my master's course work and thesis. The resources provided by MNSU were of course crucial for the building and testing of the project.

I would also like to thank my wife Adriana for the unconditional support she provided while balancing my work and school life. This would not have been possible without her patience and care.

This page was left blank intentionally.

Chapter 1 : Introduction

This chapter will view techniques that can be used in the control loop of three phase inverters. Among these controls is the model predictive control (MPC) which will be a focus in the thesis.

1.1 Background

Distribution generation (DG) systems are becoming more popular because of price fall in renewable energy components [1] such as solar power and wind turbine systems. Recent events such as the Texas grid failure of 2021 [2] displayed reliability issues in the main electric grid that could be remedied by back up DG systems at the distribution level. The problem with harvesting renewable energy sources (RES) is that the resulting electric power is in a form incompatible with the mains grid which is transported as alternating current at 60Hz. RES such as solar array produces voltage and wind power produces DC and AC voltage at variable frequencies, respectively; the inverter plays an essential role in DG integration. The rise in RES integration in recent years has made the study of inverter control increase in importance. Due to this, traditional control schemes used in industry are being implemented in power electronics and new models including machine learning techniques are being researched to meet the demand. This thesis focuses on machine learning based MPC as a possible alternative to the conventional MPC for this application.

1.2. Control Schemes for Power Converters

1.2.1 Modelling the System

Before the control schemes are discussed, a proper model of a power converter needs to be established, a three-phase voltage source inverter will be used and discussed in this paper. A popular way to represent a system is the state-space averaging (SSA) model since it uses the average state of the transistors in switch-mode power converters that are used for pulse-width modulating (PWM). The process of describing a power converter using the SSA method begins by using electrical principles to obtain the differential equations to describe the system.

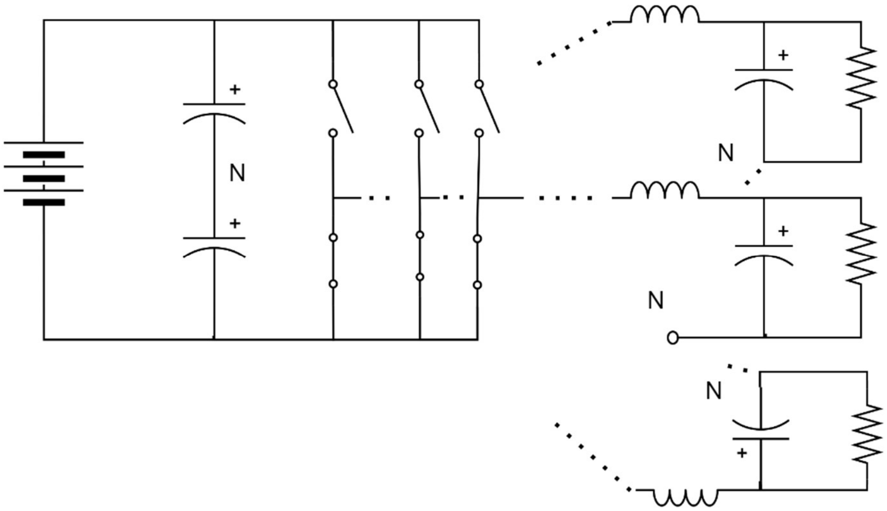

Figure 1.1: Half-bridge voltage-source inverter.

For a three-phase inverter as shown in Figure 1.1, each phase is ideally symmetrical with respect to structure and component values. This is because we want the phases to be balanced so minimal current is carried in the neutral conductor. Because of this symmetry, a single phase can describe the rest of the system by shifting the phase angle. The differential equations can be used to describe the state-space representation of the inverter which can be used to synthesize controllers. Equation 1.1 shows the state-space model for a single-phase inverter.

$$\dot{x} \; = \begin{bmatrix} -\frac{r}{L} & -\frac{1}{L} \\ \frac{1}{C} & -\frac{1}{R \cdot C} \end{bmatrix} \begin{bmatrix} i_L \\ v_C \end{bmatrix} + \begin{bmatrix} \frac{V_{dc}}{L} \\ 0 \end{bmatrix} \cdot u \qquad (1.1)$$

where $x = [i_L, v_c]$ is the monitored states and u is the duty cycle for the PWM module. Since the inverter consists of three phases, the PWM will be shifted by 120 degrees for the remaining two phases.

1.2.2 Rotational Reference Frames

The inverter outputs three phases that are separated by 120 degrees as necessary for a three-phase balanced system. These three output signals can be converted into simpler signals by using the rotational reference frames. Two popular frames transformations are the Clarke (α-β) and the direct-quadrature transformation.

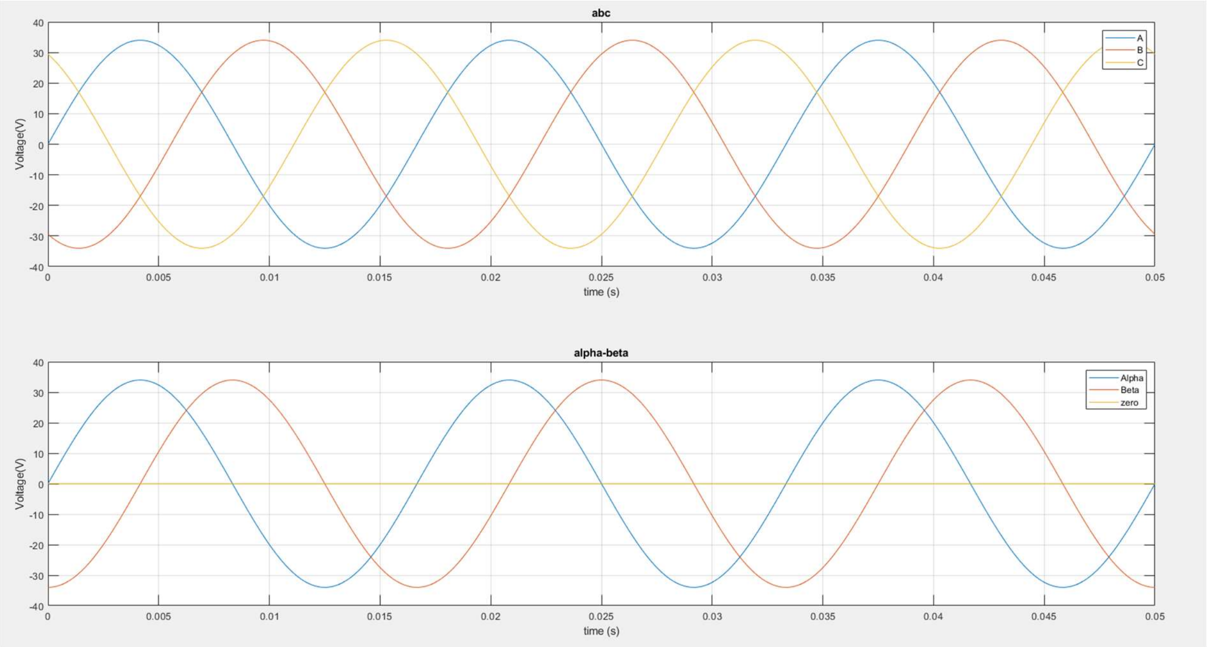

Figure 1.2: Three-phase voltages and its Clarke transform representation.

$$\begin{bmatrix} \alpha \\ \beta \end{bmatrix} = \frac{2}{3}\begin{bmatrix} 1 & -\frac{1}{2} & -\frac{1}{2} \\ 0 & \frac{\sqrt(3)}{2} & -\frac{\sqrt{3}}{2} \end{bmatrix}\begin{bmatrix} a \\ b \\ c \end{bmatrix} \tag{1.2}$$

The Clarke transform represents a three-phase system which is the standard for the electric power distribution industry in two orthogonal components. This greatly reduces the complexity of the system as it only needs one phase and its 90-degree phase shift representation. When using these signals for control purposes, the complexity of the system is reduced by changing the need from 3 controllers to 2 with a 90-degree phase delay in each one.

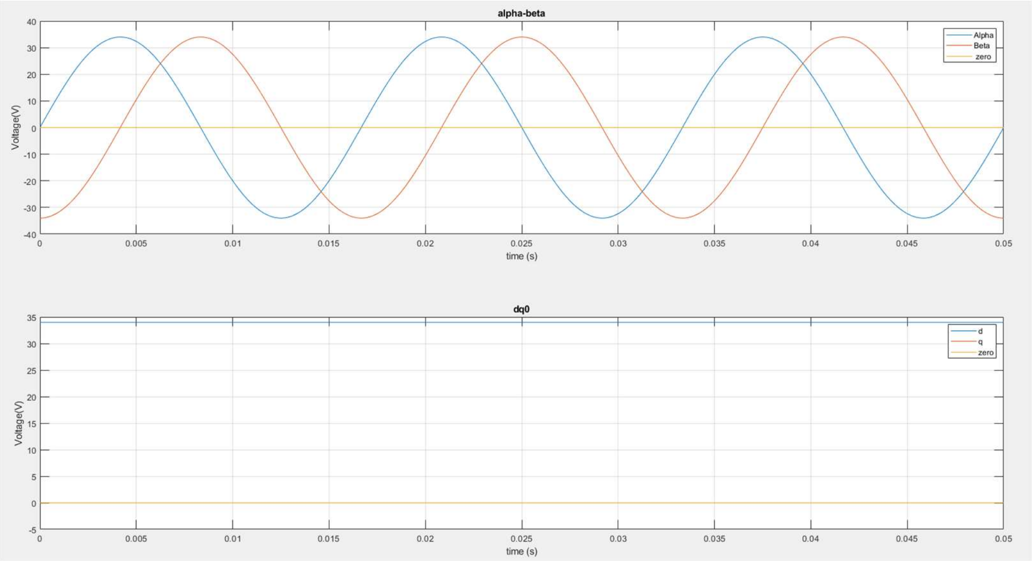

Figure 1.3: alpha-beta and DQZ transform.

$$\begin{bmatrix} d \\ q \end{bmatrix} = \frac{2}{3}\begin{bmatrix} \sin\theta & -\cos\theta & 0 \\ \cos\theta & \sin\theta & 0 \end{bmatrix}\begin{bmatrix} \alpha \\ \beta \end{bmatrix} \tag{1.3}$$

The DQ transform is a combination of two transforms, one of which is the Clarke transform. The other is the Park transform which rotates with the α-β stational frame to make them constant. This transform is particularly useful since it simplifies the control synthesis from a time varying output signal to a constant signal that is easier to track by controllers.

1.2.3 PID Control

A common control is the Proportional-Integral-Derivative (PID) controller which utilizes three components to alter the error between the reference and the sampled system's output.

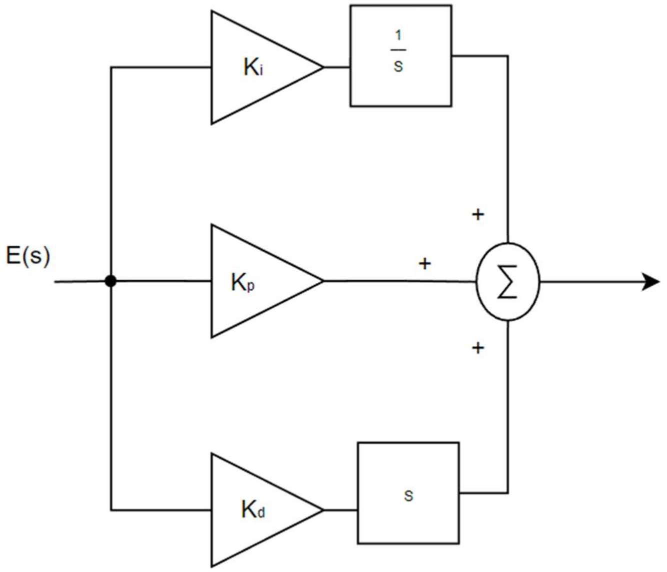

Figure 1.4: PID control structure.

In power converters, the PID is mostly used as a Proportional-Integral (PI) control by setting the derivative component to zero on the structure shown in figure 1.4. The common converter control consists of dual control loops: the outer loop is for tracking and maintaining the voltage at a certain level while limiting the current references, and the inner loop is for tracking the reference current provided by the outer loop. Digital tuning software such as MATLAB has made tuning PI controllers easy and readily available digital signal processors (DSP) modules make programming the controllers accessible.

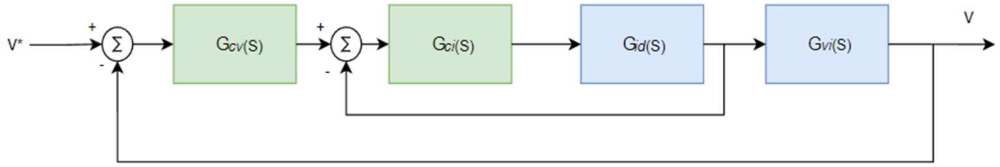

Figure 1.5: Voltage and current control loops.

The PI control can be paired with the rotational reference frame since the DQ components are constant, which further simplifies the design of the controller. The control output would then be used to control the duty cycle of switch mode converters like the inverter seen in figure 1.1.

1.3 A literature Review of the MPC

1.3.1 The Model Predictive Control

MPC has become a popular method for power electronics with the increasing computation power of micro controllers and DSPs. MPCs work by using the system's transfer function and state variables to optimize a cost function across several future sample steps. This optimization predicts the best control effort over the sample steps considered. The number of steps is called the control horizon and a longer predict horizon result in more computations to be done per sample period.

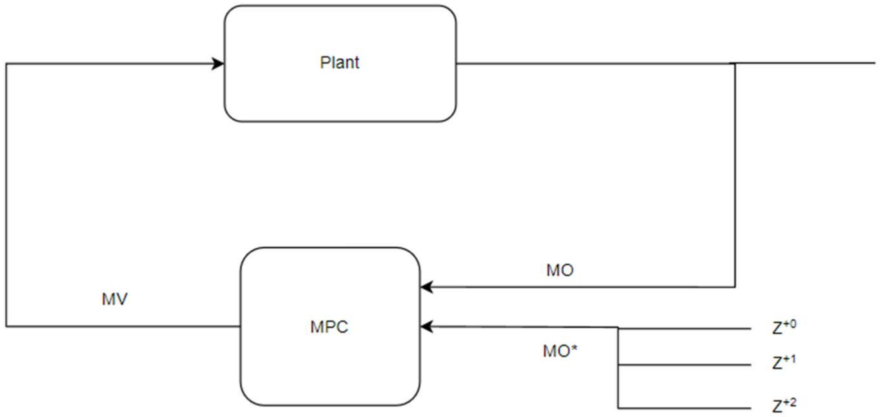

Figure 1.6 MPC Control loop with a three-step control horizon.

The MPC can use the alpha-beta reference frame for tracking the plant's output. Figure 1.7 illustrates the MPC's online optimization.

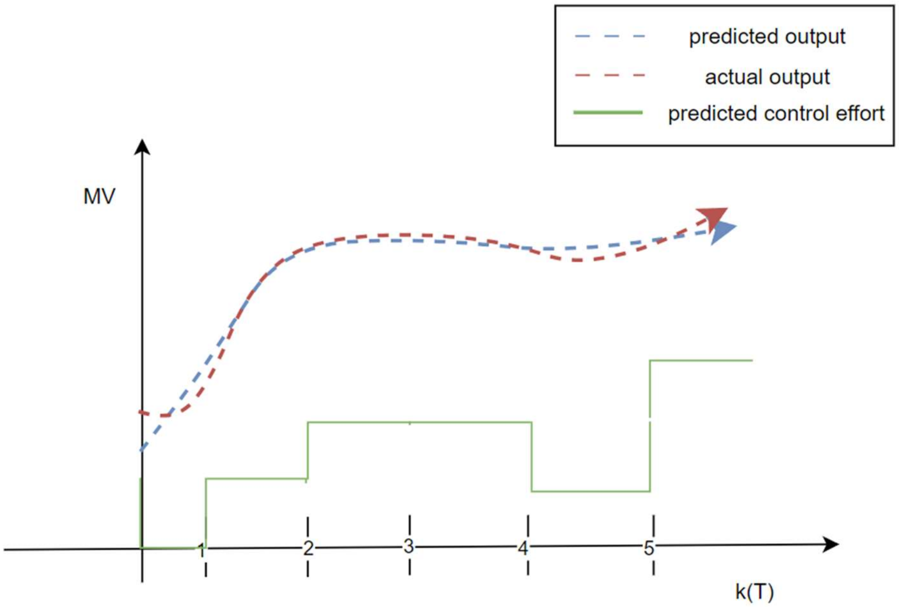

Figure 1.7: MPC online optimization in discrete time.

MPC has several advantages such as the easy inclusion of nonlinearities and constraints due to the online calculations performed every sample step which leads to good performance in three-phase inverters [4]-[6]. There are two MPC types, one is continuous control set (CCS) MPC and the other is finite control set (FCS) MPC [7]. Unlike CCS-MPC in which the switch status is varied in each period, the FCS-MPC only considers a finite set of states and switches status within entire sampling period is either on or off, which greatly reduces prediction states. However, the CCS-MPC has better performance than the FCS-MPC.

1.3.2 Cost Function and Optimization

Various MPC algorithms propose different cost functions to obtain the control law [4]. The cost function typically includes the differences between the reference signal and the sampled output (also called the error), and the control effort which is the rate of change of the input control output over the control horizon; they are organized with different weight. Along with constraints to inputs, outputs, and horizons, the tuning of an MPC consists of parameter optimization. The traditional objective can be expressed as follows:

$$\min J = \sum_{j=1}^{h} \left[w_e \cdot |e(k+j)|^2 + w_u \cdot |\Delta u(k+i-1)|^2 \right] \tag{1.4}$$

where the error term $|e(k+j)|$ can be considered as the difference between the reference and the predicted values of the output; $\Delta u(k+i-1)$ term indicates the rate of change of the control input across the control horizon. It should be noted that the rate change of the control actuation can be subject to constraints which are considered when optimizing the problem. These constraints can be used to limit the control's output extrema and rate of change per sample interval.

1.3.3 Disadvantages

One of the main disadvantages of the MPC is the dependence on the system model in which there is load and parameter uncertainty. Other phenomena like faults, quick changes in loading, or nonlinear loading could affect the performance since the state predictions are based on a pre-configured plant model.

Another disadvantage is the high computational cost due to an online optimization problem within every sampling interval. These challenges are the main motivation for exploring and comparing other controls to the MPC.

Chapter 2 : Literature Review of Machine Learning Based MPC

This chapter gives a brief introduction to machine learning like artificial neural networks (ANNs) and support vector machines (SVMs) which use data from a controller to perform a curve fit that can be used in a control loop for a three-phase inverter. The controller's optimization occurs offline in contrast to the online optimization of the MPC. This thesis explores if offline optimization can achieve better performance than a online MPC when a machine learning based MPC is used.

2.1 Machine Learning Based MPC

Two machine learning techniques, the ε-SVM and the Radial Basis Function-Artificial neural network (RBF-ANN) are the methods used and compared in this thesis. SVM has been found to be a more efficient method [9] in certain applications which is essential when working within the limits of widely used DSPs. The following sections will explore these two methods and their operation.

2.1.1 Structure

The RBF-ANN is an artificial neural network which is trained with an activation function that takes the form of a radial basis or gaussian curve. The ANN training algorithm uses gradient descent which attempts to find a minimum in error between the model's output and the training output values; this would produce a response that models the training input and output [9]. ANN-MPC has historically been the method of choice when considering power electronics machine learning based control models [10]-[12].

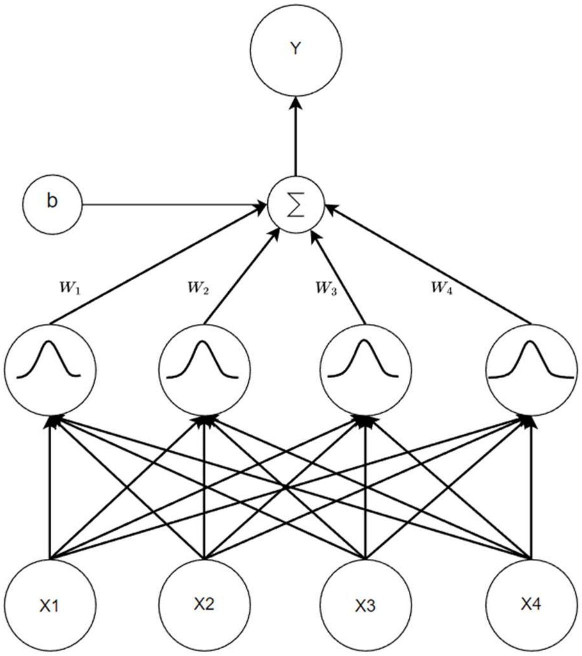

Figure 2.1: ANN architecture.

The figure above shows how the inputs interact with the ANN parameters to sum up to an output. The relationship between the input and output can be expressed by the following:

$$Y = \sum_{i}^{n} w_i \cdot \phi(x, c, \sigma) + w_0 \tag{2.1}$$

The relationship above shows how the output is a sum of weighted inputs plus a bias. The weights are part of the activation function, and they depend on parameters corresponding to the nature of the activation function. As an example, a radial basis function (RBF) will have a spread and a center or mean associated to it. The mean and spread can be derived from the dataset collected for training. It's important to note that while ANNs are very good at imitating systems they are limited by the samples given, i.e., an ANN would not do well for new samples that was not learned.

The SVM gets its name from the support vectors that make up its performance. These support vectors interact with the input and add together to create the output that best fits the trained output. SVMs have been traditionally used in classification and regression problems such as face recognition. As a control system, the SVM is used as a regression tool that fits the relationship between the input and output in a higher dimensional space. The ε-SVM mapping function describes a hyperplane that separates the data in a higher dimensional space with a plane. $\tilde{u}_k = w^T \cdot \varphi(\mathrm{X_k}) + b$

(2.2)

where w^T represents the normal vector to the hyperplane, $\varphi(X_k)$ indicates the SVM's kernel or activation function, and b is the bias or offset. Figure 2.2 shows the linear relationship in the higher dimensional space which can easily separate the points. The linear separation in high dimension is equivalent to nonlinear separation in low dimension.

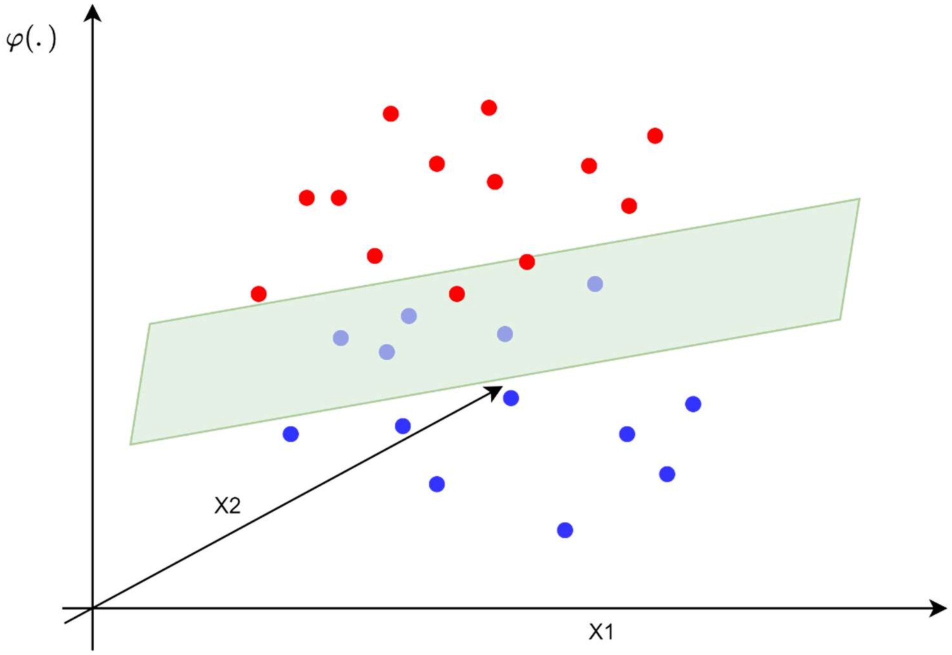

Figure 2.2: SVM hyperplane

This separated data can then be used to create an error margin using a distance called the epsilon margin or ε-tube. The samples inside the tube are said to have no error while the samples outside are called the support vectors. A tube of zero distance is called a hard margin SVM and it can cause problems since it regards all samples as erroneous, and the optimization can cause overfitting that losses generalization. For this reason, in this thesis, a soft margin SVM will be used meaning that there will be a greater than zero epsilon value leading to a reduced number of support vectors along with computational cost, and greater generalization.

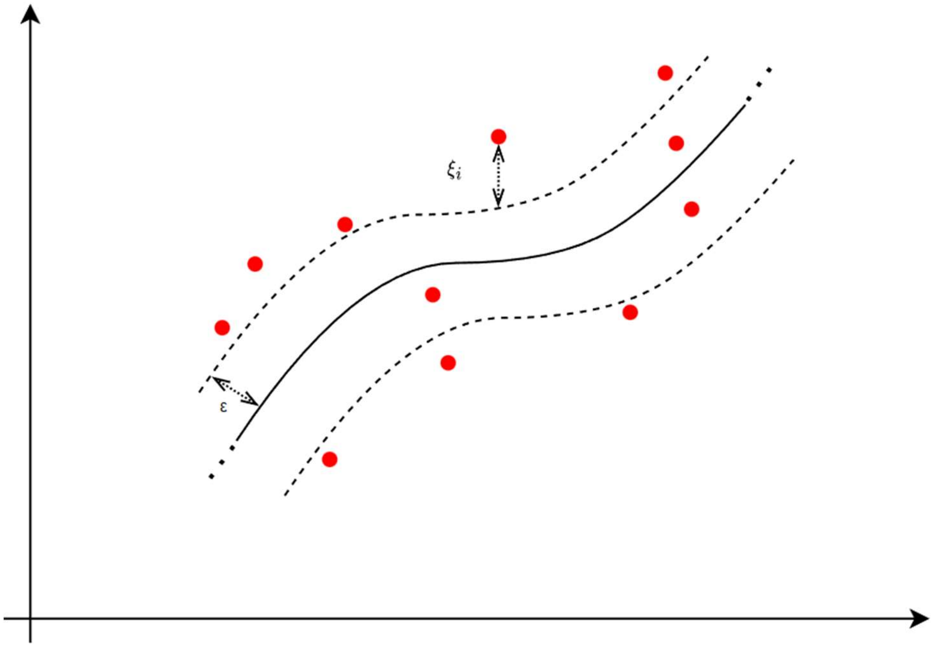

Figure 2.3: Epsilon tube.

Given the that the error samples are defined as those lying outside the ε-margin, one can use this margin and the orientation of the hyperplane to optimize the performance of the SVM. This takes the form of:

$$\mathrm{Min}\frac{1}{2}w^T w + \gamma \sum_{k=1}^{n} (\xi_{\mathrm{k}} + \xi_k^*) \tag{2.3}$$

$$s.t.\begin{cases} u_k^* - w \cdot \varphi(X_k) - b \leq \ \xi_k^* + \varepsilon \\ w \cdot \varphi(X_k) + b - u_k \leq \ \xi_k^* + \varepsilon \\ \forall k\colon \ \xi_k, \xi_k^* \geq 0 \end{cases} \tag{2.4}$$

Positive Lagrange multipliers are used in formulating the optimization problem and introducing variables ξ_k , $k = 1,2, \ldots, n$ allows us to flex the error margin for problems like controls [8]. The non-zero terms ξ_k and ξ_k^* then become support vectors in the regression model which are used to program a controller.

2.1.2 Data Preprocessing

Training a neural network can vary on efficiency depending on the data it is given. As stated in the previous section, some parameters depend on the activation function or kernel which can be derived from the training set. Normalizing the input and output is a simple yet effective way of improving performance in training. Because inputs could be of different scales such as voltage and current, normalizing the input prevents the voltage from having a greater influence on the output since in general it will be a larger value. Proper format is another important factor in preparing data since the input should be in a format that represents the model and can be fed into the training vector. The output vector should also be in a format that can be compared to an ideal output for analysis.

2.1.3 Training and Fitting Performance.

Training data should include a complete scope of the inputs that are possible for the system to encounter. SVM controls can be more general if the soft margin SVM mentioned is employed. This only happens if there is no overfitting during training. Overfitting occurs when the SVM is forced to fit a curve with strict constraints and an excessive number of hidden units. A balance must be reached during training to avoid getting a system with very large amounts of hidden units despite the low error. Figure 2.1.5 below shows how a sinusoidal curve can fit a data set with a seemingly linear trend. Both line and the sinusoid shown could have similar errors when fitting the curve. A low number of support vectors is also desirable because it would reduce the resources needed for the application.

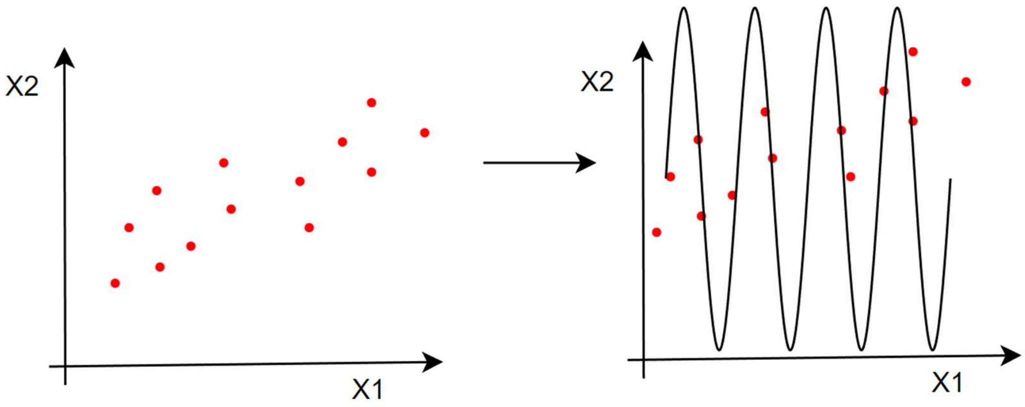

Figure 2.4: Overfitting of the SVM.

To compare the effectiveness of the methods, controllers will be compared in different aspects such as total harmonic distortion (THD) in the output, dynamic loading, and computational loading [14]. The Machine learning controllers are expected to perform similarly to the MPC but using less computational resources.

Chapter 3 : Simulations

In this chapter, simulation studies and results will be described. The methods and parameters used for the simulations were picked to model the three-phase inverter described in chapter 1. For this thesis, MATLAB/Simulink environment was used to model and design controls and later as a programming tool for the controller used during testing. The results from the simulations are used to set expectations for the controllers performing on hardware.

3.1 Simulation Studies

The first step is to use a script including the inverter parameters and state-space average model to design the MPC which will be served as the reference controller in this thesis. Using MATLAB's "mpcdesigner", an MPC Simulink model was created with small prediction and control horizon to minimize computational loading. Figure 3.1 shows MPC designer while creating the controller and testing a sinusoidal response.

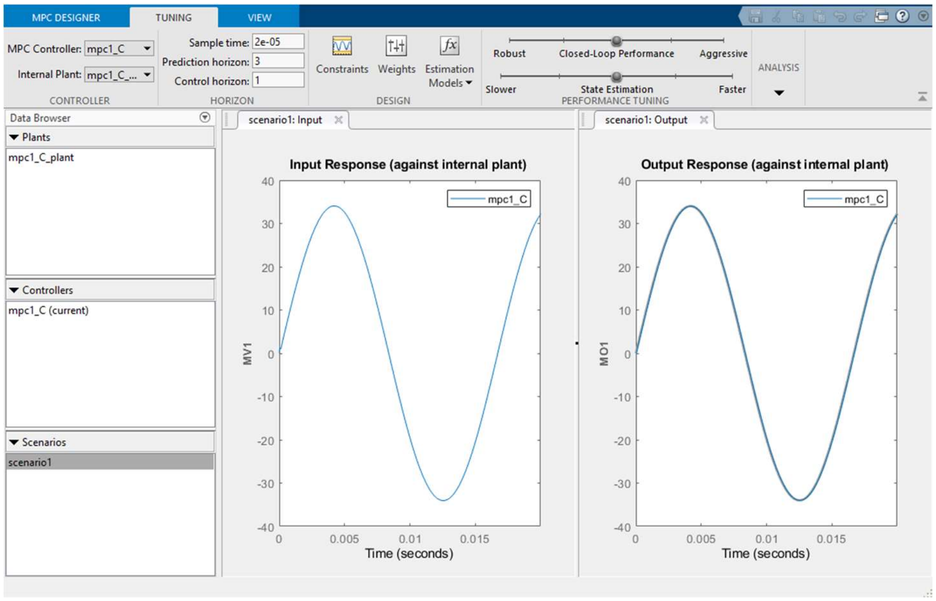

MPC Controller: mpc1_C

Internal Plant: mpc1_C_...

Sample time: 2e-05

Prediction horizon: 3

Control horizon: 1

Figure 3.1: MPC design tool.

A Simulink model was then created along with the plant to output the voltage needed to simulate the control loop. The sampling time of the control was set to be the same as the switching period which was 20µs. Similarly, the L-C filter and power supply were set the same as the nominal values for the inverter. Figure 3.2 shows the inverter control loop used for estimating the MPC’s performance.

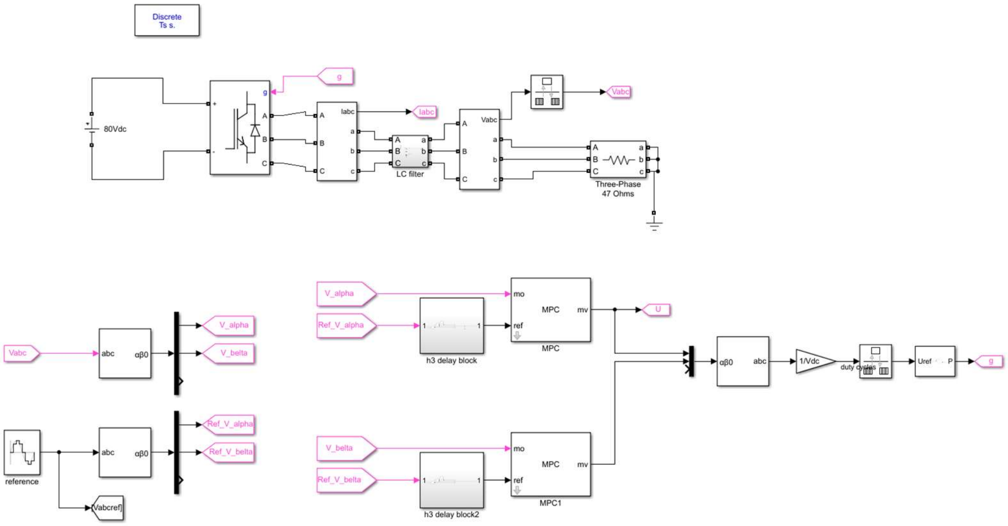

Figure 3.2: Inverter and MPC control loop.

The THD, power factor, and reference tracking were observed in the simulation using scope tools and were deemed acceptable when the THD was below 5%, pf was close to unity, and the reference error was less than one percent. When the MPC has good performance, it could then be used to gather data for training the SVM and ANN as illustrated in the previous chapter. The following figures show the MPC's three-phase voltage with each reference phase, the THD as measured by a THD block and the phase A current under a 47 Ohm load. The error is also shown to be around 1.2V maximum between the alpha voltage signal and the reference.

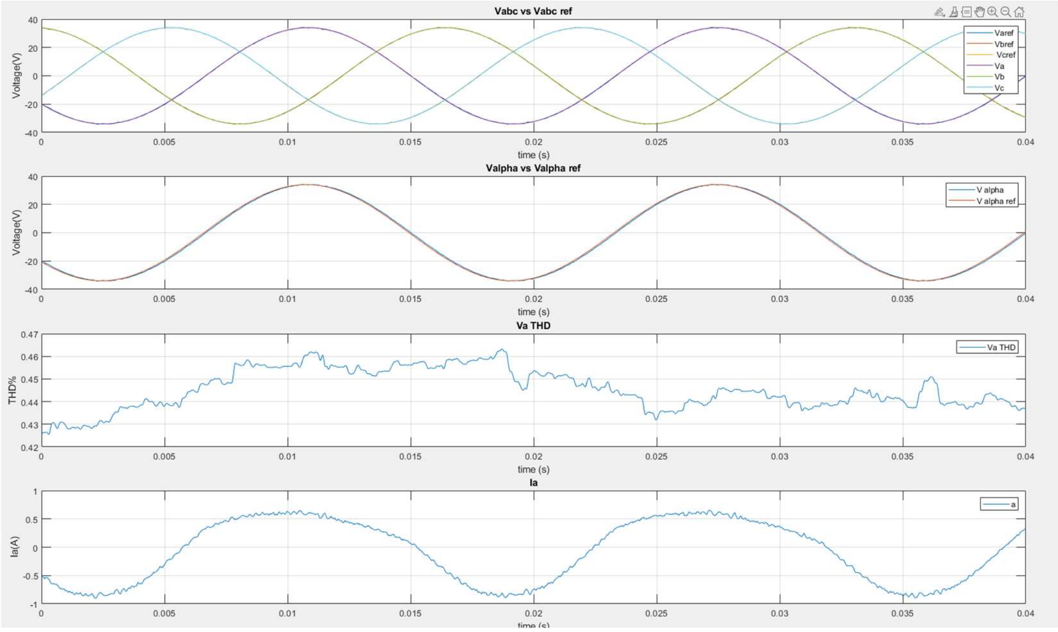

Figure 3.3: MPC performance.

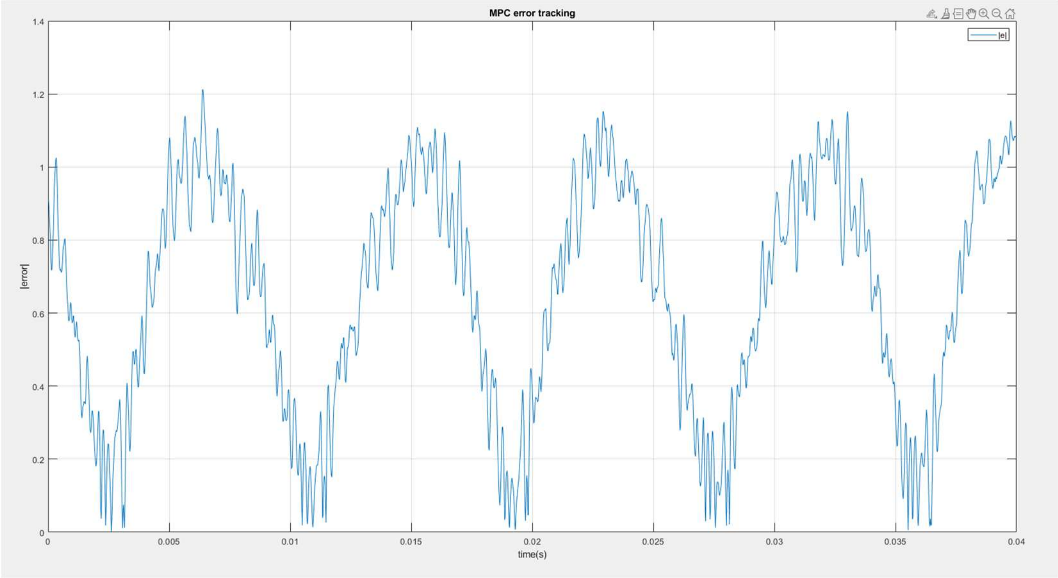

Figure 3.4: MPC error tracking.

As seen in chapter 2, the SVM and ANN require data from the system they are to imitate. For this purpose, 10,000 samples were collected from the simulation generated by the tuned MPC. In this case, the input would be the three stepped future references and the alpha quantity representing the three-phase voltage quantities. The output is the control's effort on the plant is also recorded as the relationship between the input and output will be mapped by the controller when training.

To optimize the SVM training, the error and THD landscape was created to see what combination of parameters synthesized the best controller. Figure 3.5 shows the THD magnitude vs SVM parameters. The figure also shows the magnitude of absolute error as the parameters swept using a color gradient. As seen in the graph, the best combination of parameters lies near 25 kernel scale.

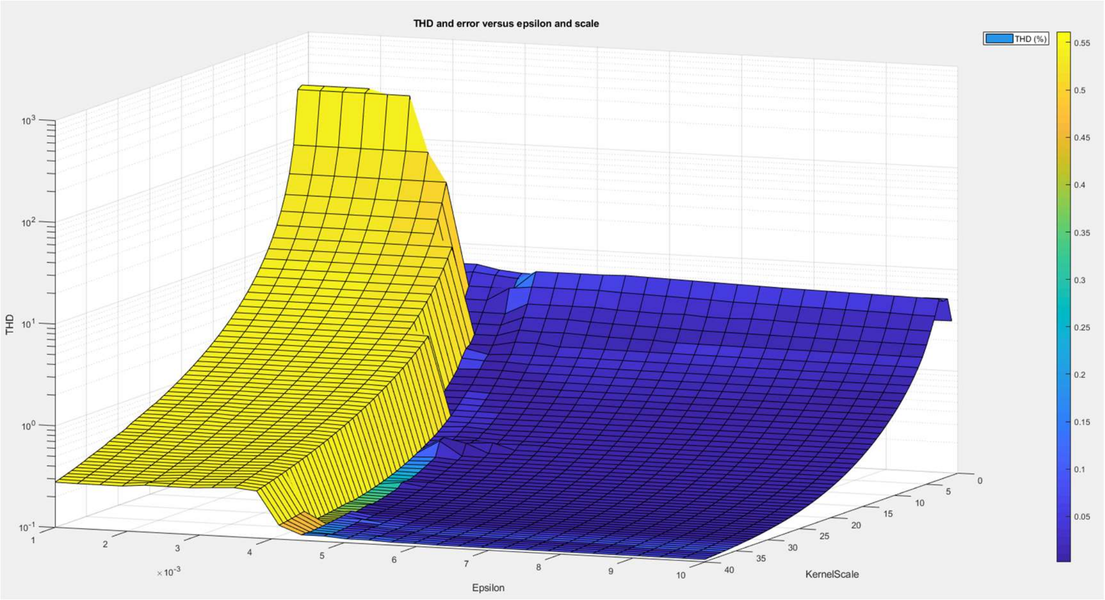

Figure 3.5: THD and error versus SVM parameters.

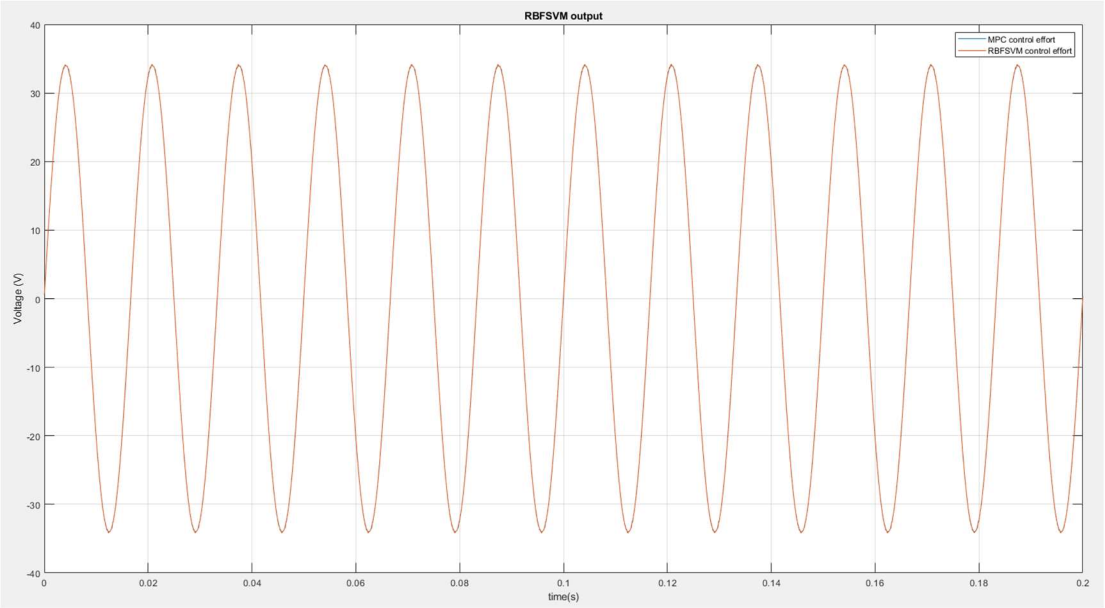

Figure 3.6: RBFSVM-MPC outputs and reference.

Using the parameters obtained from figure 3.5 the RBF-SVM-MPC was synthesized. This control needed to perform like the MPC with the same input being three future stepped references and the inverter voltage measurement. Figure 3.6 shows the control's response versus the MPC's response overlapped. The error between the training output and the RBF-SVM-MPC output was observed to be less than 0.01V. Figure 3.7 shows the absolute error between RBF-SVM-MPC's prediction and MPC's prediction seen in figure 3.6.

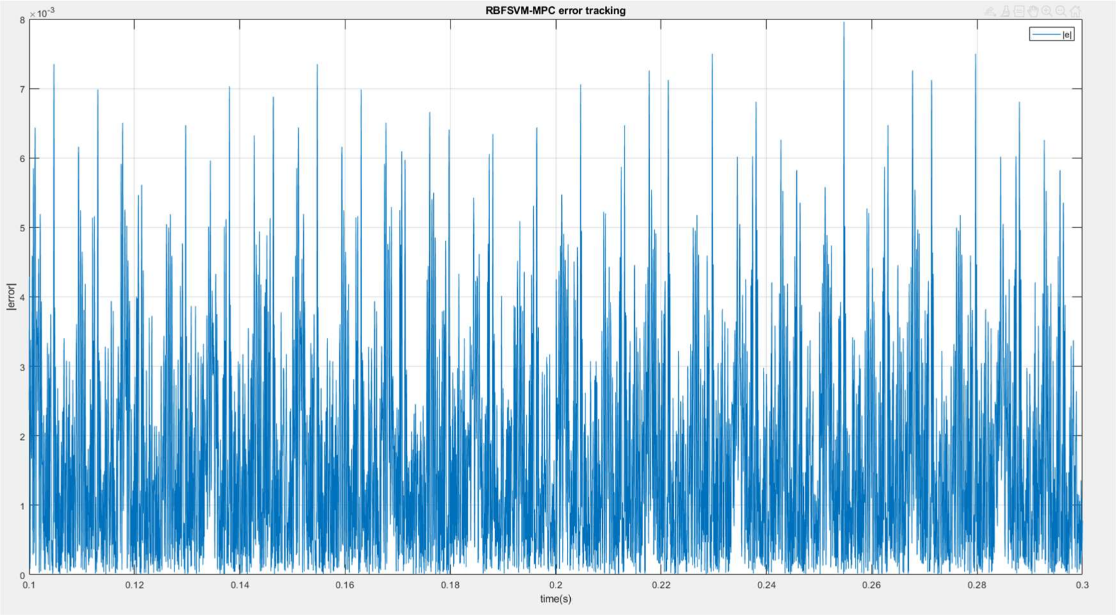

Figure 3.7: RBF-SVM-MPC error tracking.

The RBF-SVM-MPC control loop was very similar to the MPC's with the only difference being the control getting replaced by a set of operations that perform the kernel trick on the input and implement the prediction. Normalization and denormalization is also present within the block since the trained control needs data in the same shape that it was trained with.

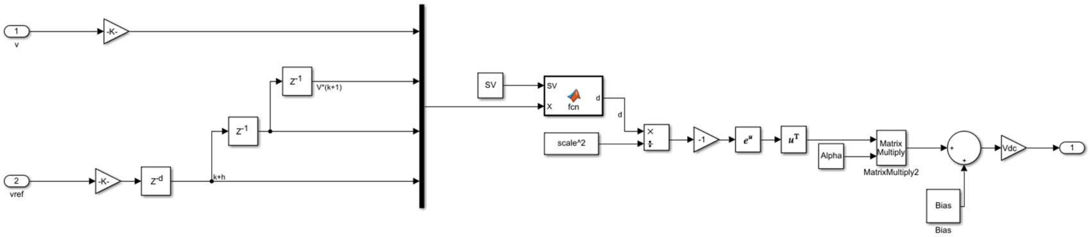

Figure 3.8: RBF-SVM-MPC controller block.

The ANN-MPC was trained using the same spread and hidden units to compare the performance of both machine-learning based controllers. Having the same number of hidden units will also make it easier to compare computational loading of controllers. Figure 3.9 shows the ANN controller as implemented on Simulink. Figure 3.10 shows the training performance versus epochs that resulted in the controller used in this paper.

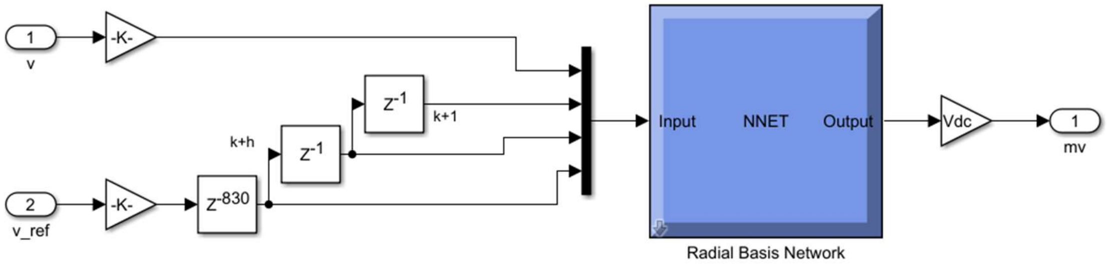

Figure 3.9: ANN Simulink model.

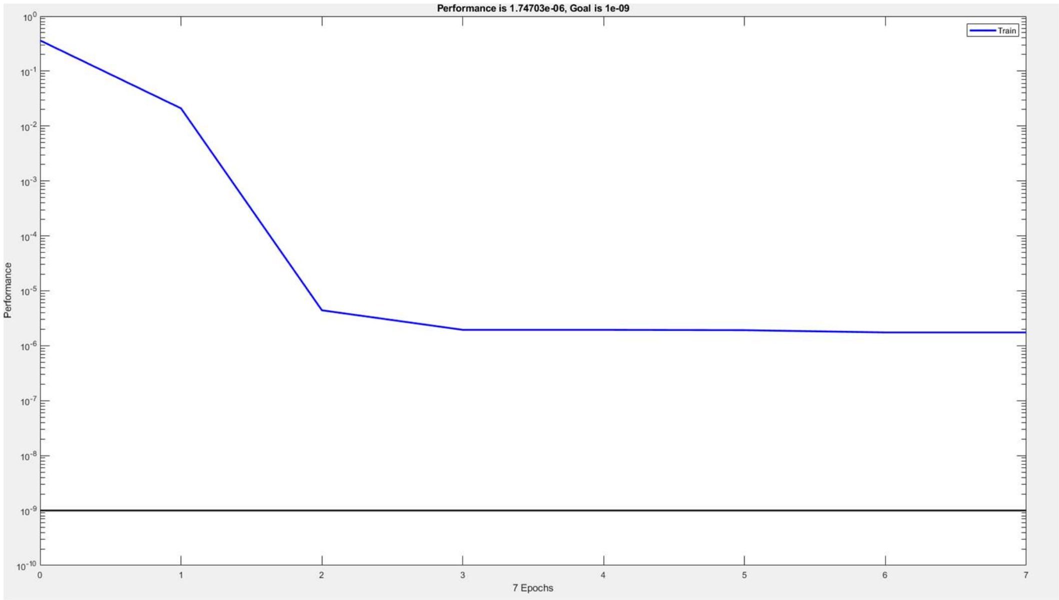

Figure 3.10: ANN training.

The MAE between the training data and the network’s output was observed to be at 0.01.

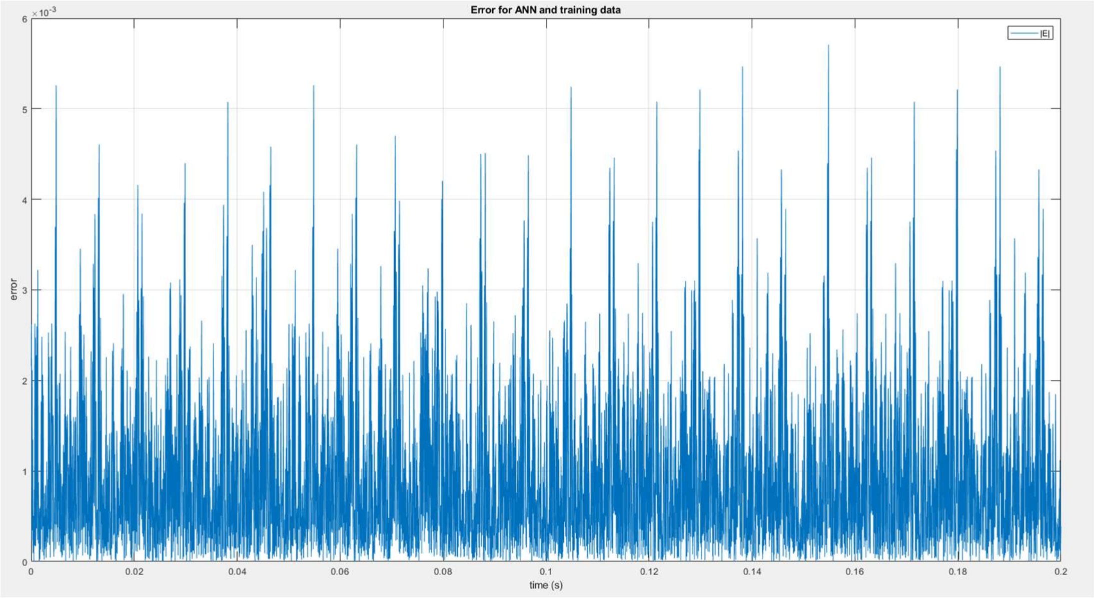

Figure 3.11: ANN training data error.

This performance only shows how good the models are at fitting the training data not how the model reacts as a control in an actual control loop. For this the controls were simulated using the inverter model seen in previous chapters.

3.2 Simulation Results

For comparing performance of the three controls, simulations with varying load and model parameters were performed while measuring error and total harmonic distortion. The load was changed from the trained 47Ω linear load to a lower 32Ω linear load. A sudden change in load was also performed to see how good the controls are at tracking. The controls' response to a nonlinear load like those present in computer power supplies and other modern loads is also tested. Lastly, a change in model parameters such as the inductor and capacitor values were done to test the controls' generality.

3.2.1 Steady-State Linear Load

The three controllers were simulated using the same 47 Ohm impedance used during design and training and a 32 Ohm impedance to see the effects of a load change on the control loops seen in figures 3.2, 3.8, and 3.9. The following figure shows the harmonics components up to 6 kHz for all three controls. The magnitude is displayed in logarithmic scale to show as much of the harmonics as possible.

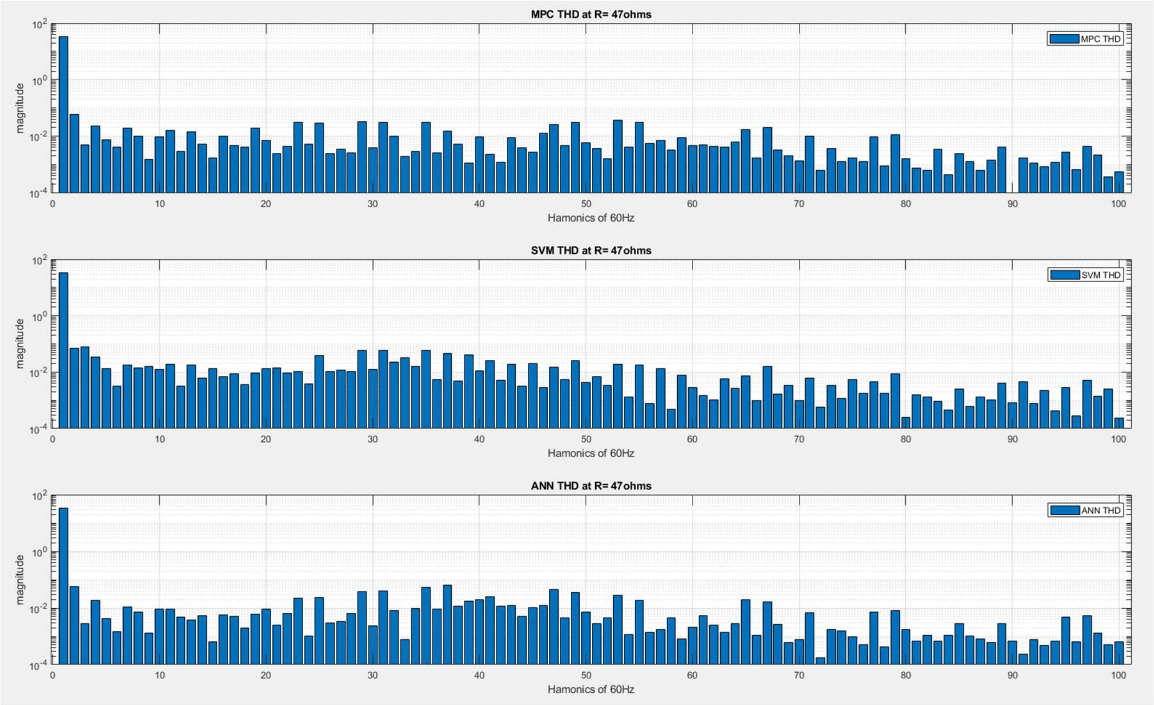

Figure 3.12: THD comparison between the three controls.

The error tracking was also plotted using the same data and the MAE (Mean Absolute Error) was calculated to assess performance and compare. Figure 3.13 below plots the absolute error over the span of 300 milliseconds at steady state operation. The resulting MAE values for the controllers being shown in figure 3.17.

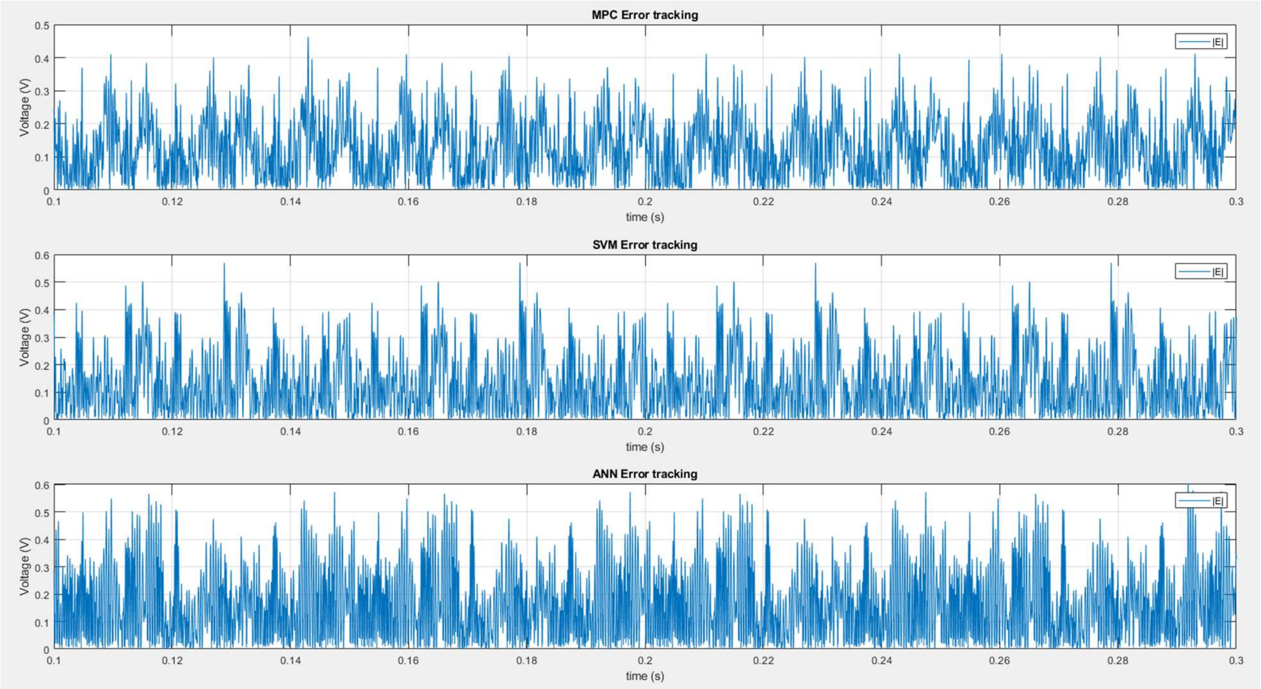

Figure 3.13: Error tracking at 47 Ohms.

Next the load impedance was changed to 32 Ohms to observe the control's response to loads that differ from the training data. Data from the simulation was extracted and the THD was then calculated. Figure 3.12 shows the harmonics for this scenario and figures 3.16 shows the THD values.

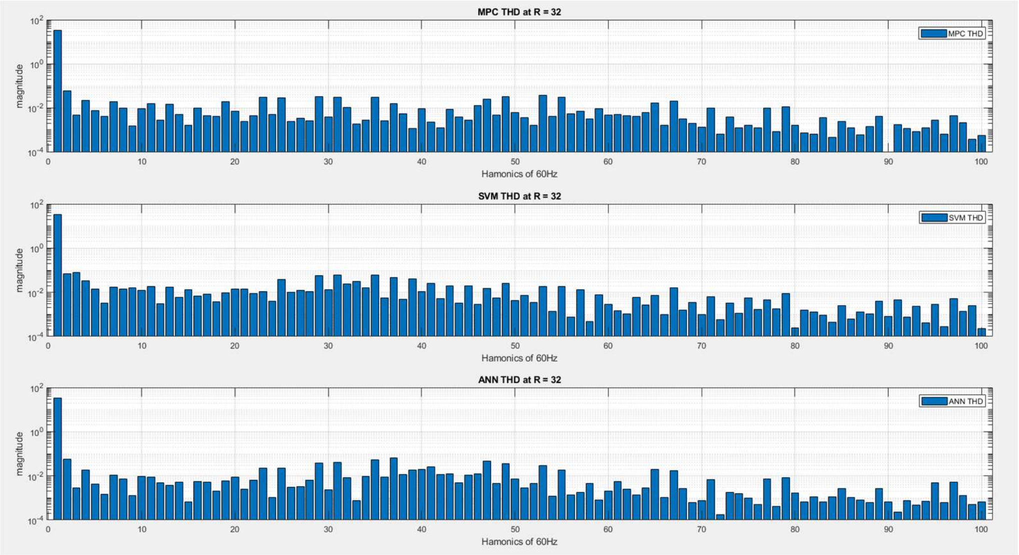

Figure 3.14: inverter THD at 32 Ohms load.

The absolute tracking error from figure 3.13 was used to calculate the MAE and was recorded for comparison.

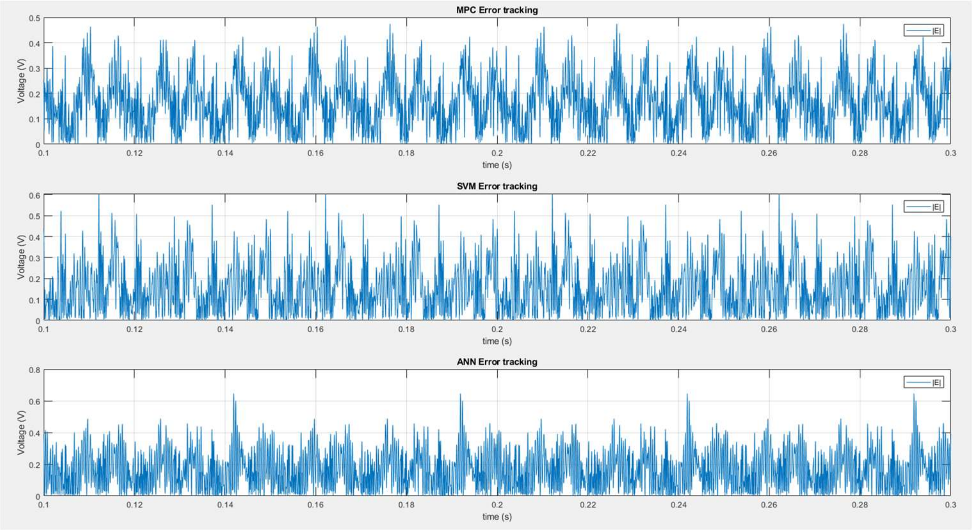

Figure 3.15: Controls’ error at R = 32 Ohms

Figures 3.16 and 17 display the THD and tracking error of the three controllers for comparison purposes. For the baseline load, the MPC outperforms the machine learning based controllers, but all controllers fall below 1% THD. As per IEEE 519, the THD recommended for grid connected devices must be below 5% [13]. This standard will serve as an acceptance threshold during this thesis; if a control is above this threshold, it can be said that it is not acceptable.

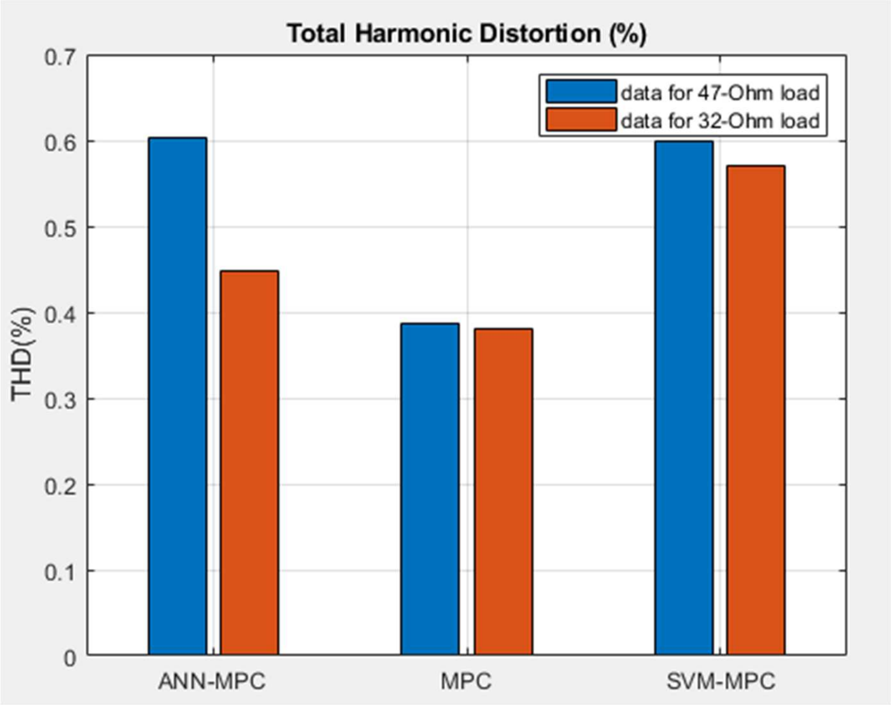

Figure 3.16: Simulated THD performance with a linear load.

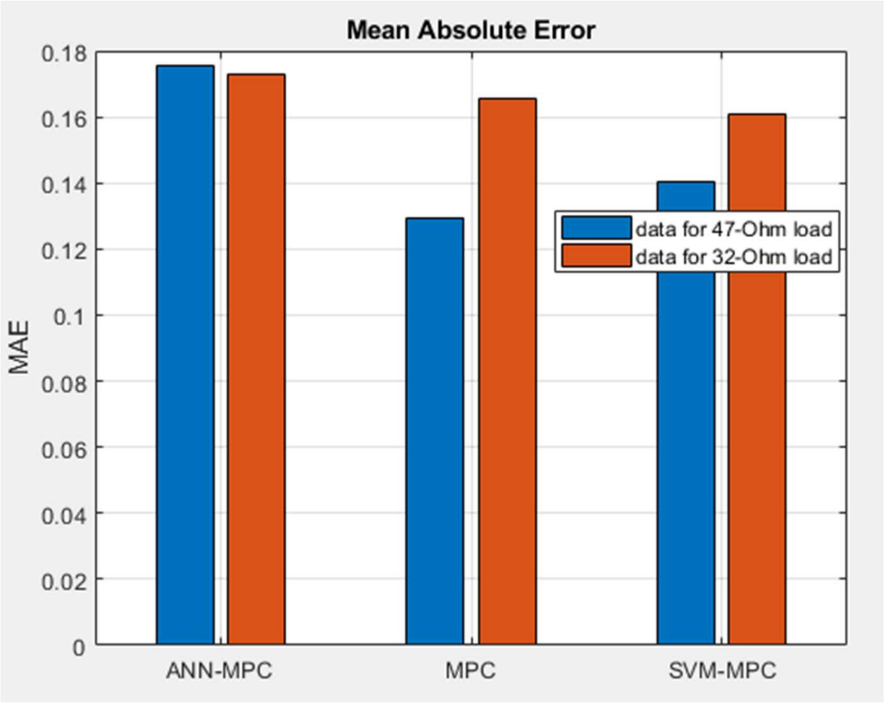

Figure 3.17: Simulated tracking error with a resistive load

3.2.2 Dynamic Loads

For the change in load experiment, a three-phase breaker was set up to close at 200 milliseconds during the simulation. A change in current should then be seen due to the lower load resistance. The control's response to this change was collected and plotted. Figure 3.18 shows the Simulink model used for this simulation.

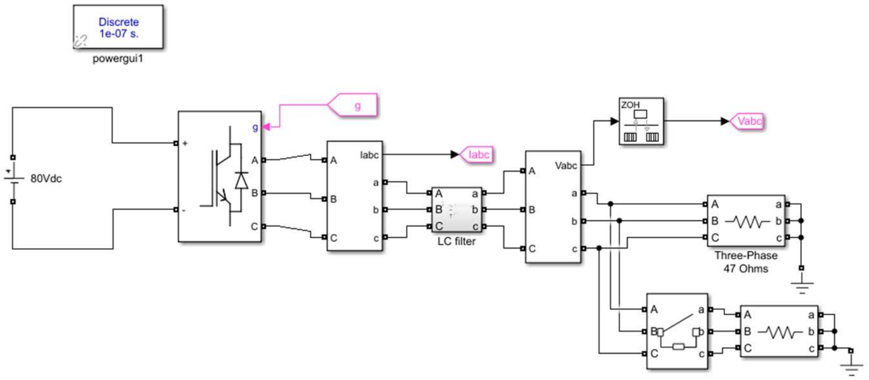

Figure 3.18: Dynamic load Simulink set-up.

The following figures show the load switch in a 200-millisecond window.

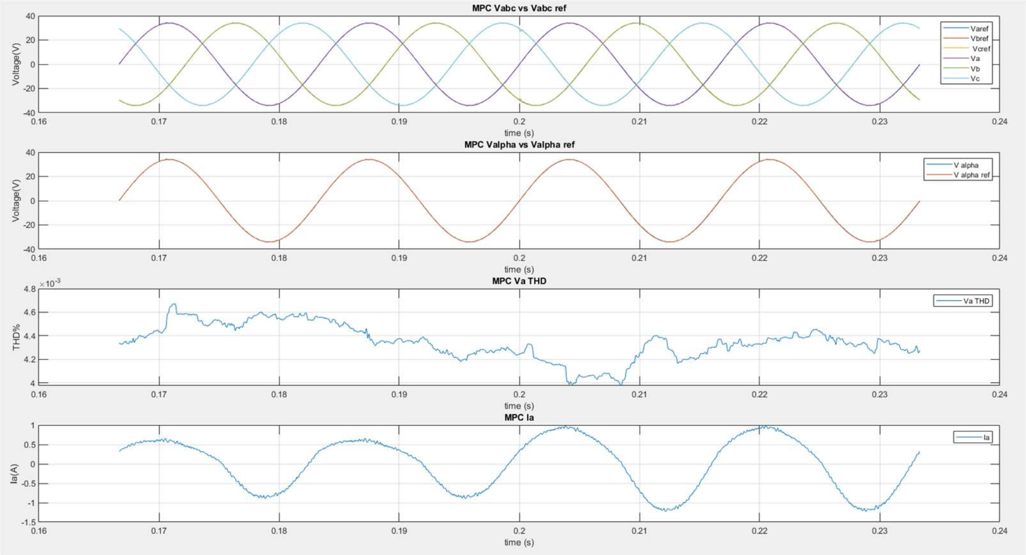

Figure 3.19: MPC performance during a sudden load switch.

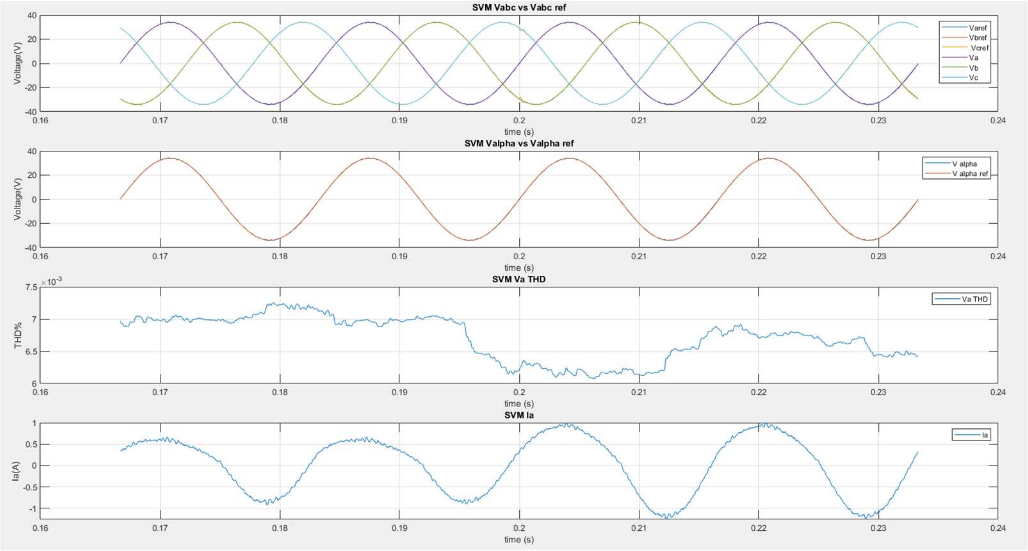

Figure 3.20: SVM performance during a sudden load switch.

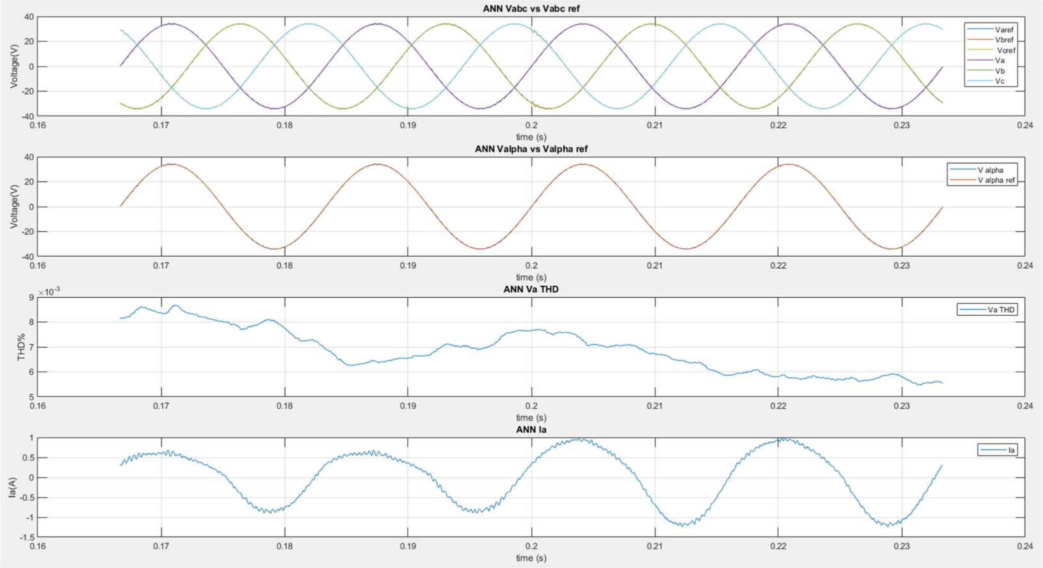

Figure 3.21: ANN performance during a sudden load switch.

Where the switch in load occurs at 0.2 seconds a sudden increase in current is seen as expected. The performance of all controllers doesn’t change much, which is a good sign that the controllers can operate during different load conditions. This is also a good indication that the machine learning controllers behave like the MPC.

3.2.3 Steady-state Nonlinear Load

For the nonlinear load experiment, a three-phase switch with an RLC network was used to act as a nonlinear load. With the input signal shut-off the free-wheeling protection diodes acted as a three-phase rectifier. Paired with a capacitor and inductor to maintain power factor on the resistive load. Figure 3.18 shows the Simulink model that would replicate this.

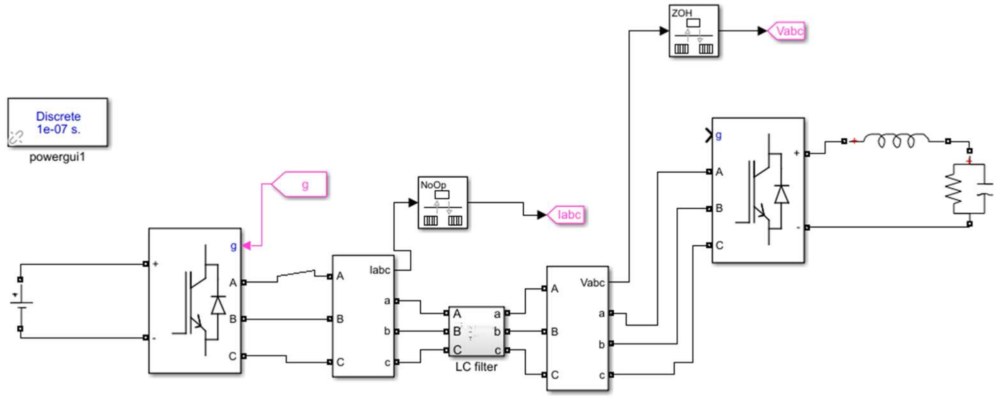

Figure 3.22: Nonlinear load Simulink model.

The three controllers were placed in the control loop for the model in figure 3.18. A portion of the steady-state waveforms were plotted like the linear load scenarios. The following figures show the waveforms plotted for the three controllers.

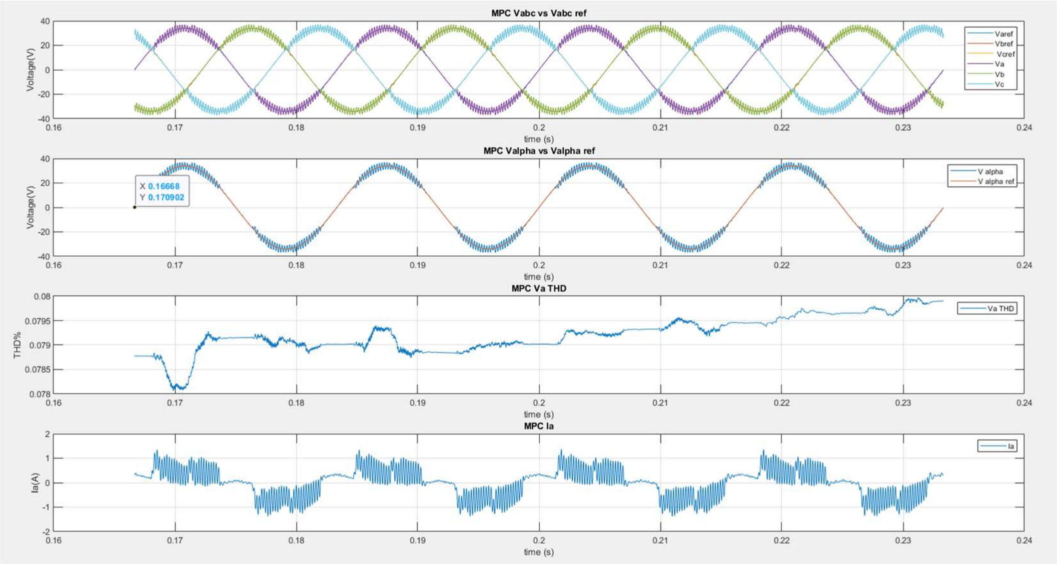

Figure 3.23: MPC performance to nonlinear load.

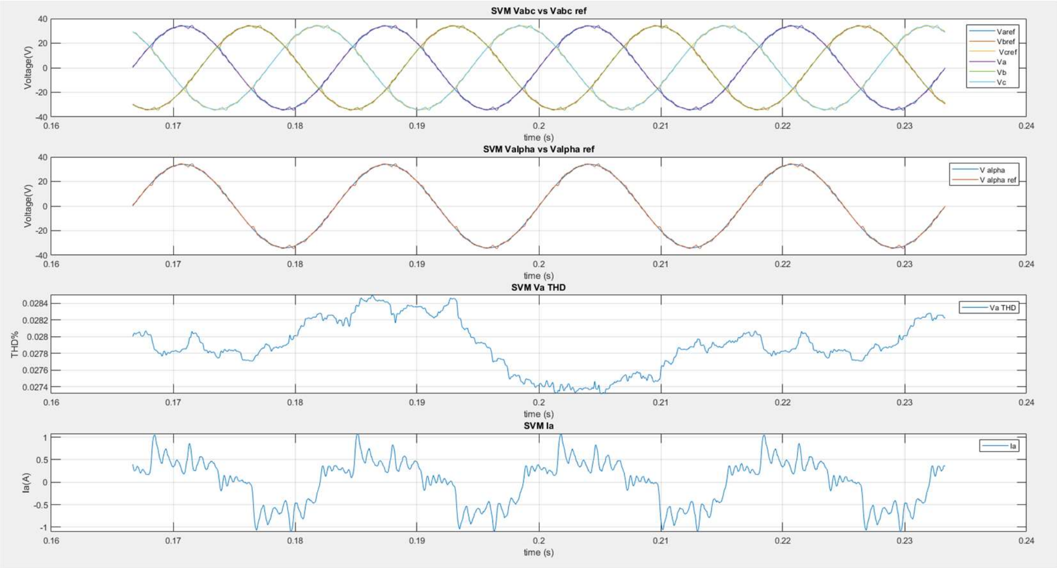

Figure 3.24: SVM performance to nonlinear load.

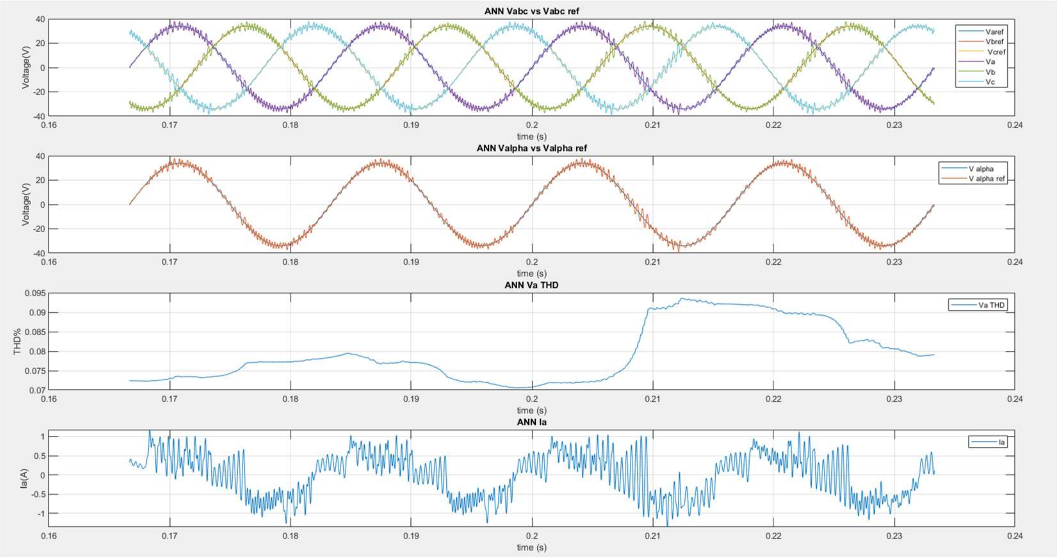

Figure 3.25: ANN performance to nonlinear load.

The total harmonic distortion and tracking error was calculated from the data in the previous figures for comparison purposes. Figure 3.26 displays the harmonic components up to 6kHz for all three controllers. The THD for the controllers in this simulation was recorded.

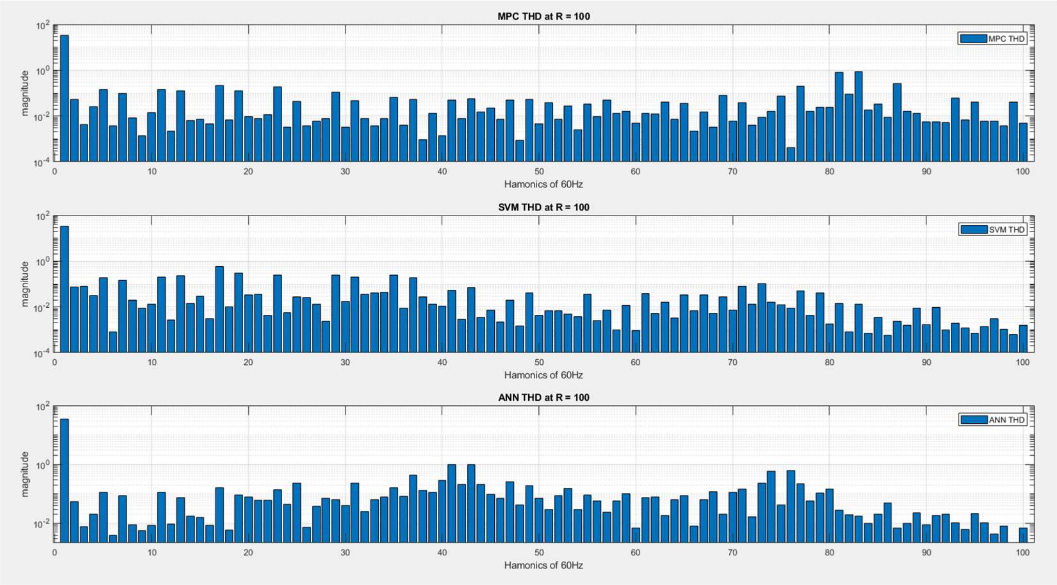

Figure 3.26: Controllers’ THD for nonlinear loading.

The tracking error plotted in figure 3.27 and the MAE is recorded and a comparison is plotted in figure 3.28 and figure 3.29.

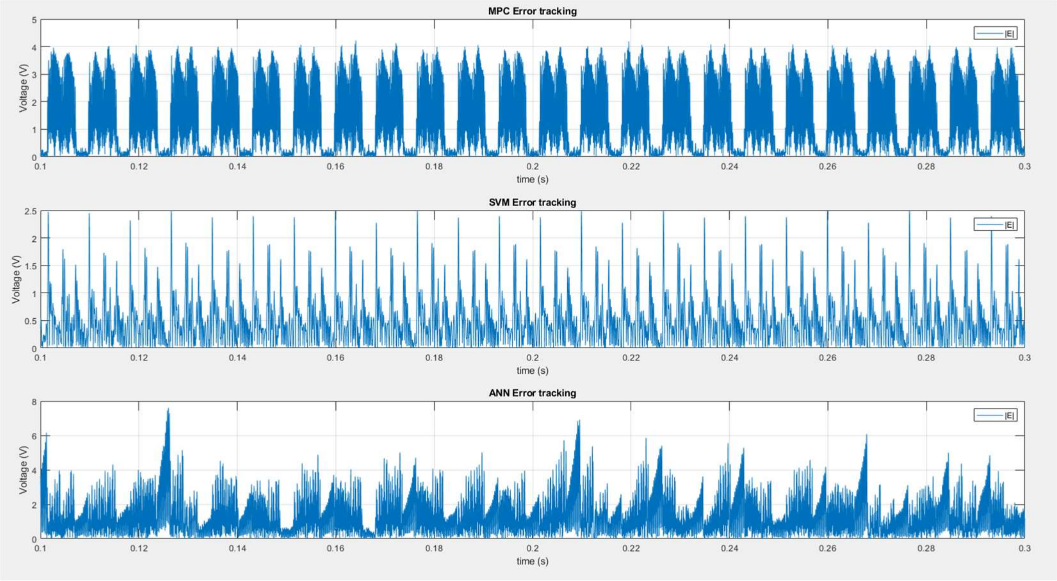

Figure 3.27: Controllers’ tracking error for nonlinear loading.

From figures 3.28 and 3.29, the ANN-MPC's performance is better in terms of THD and tracking error.

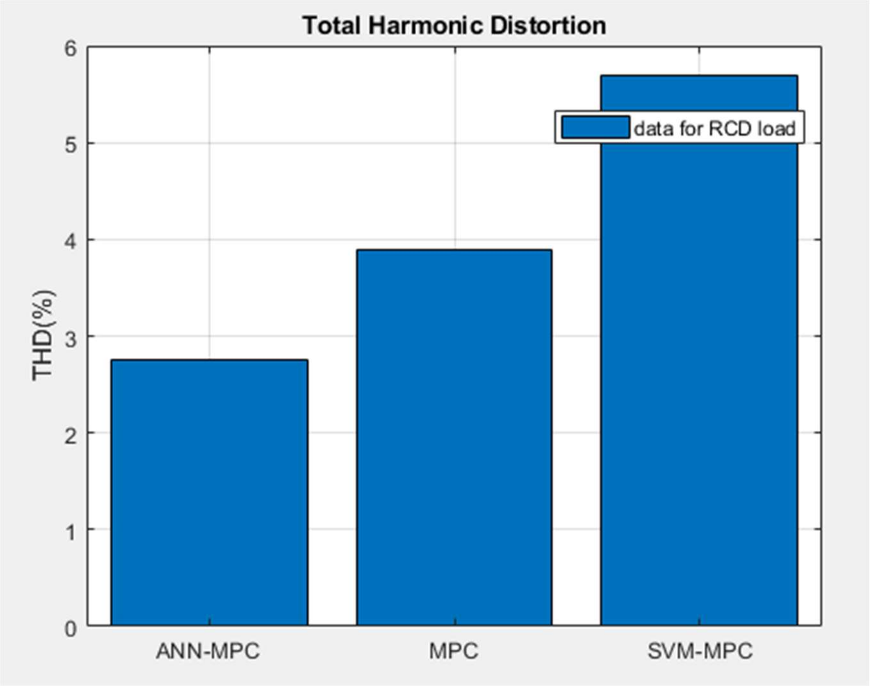

Figure 3.28: Controllers' tracking error for nonlinear loading.

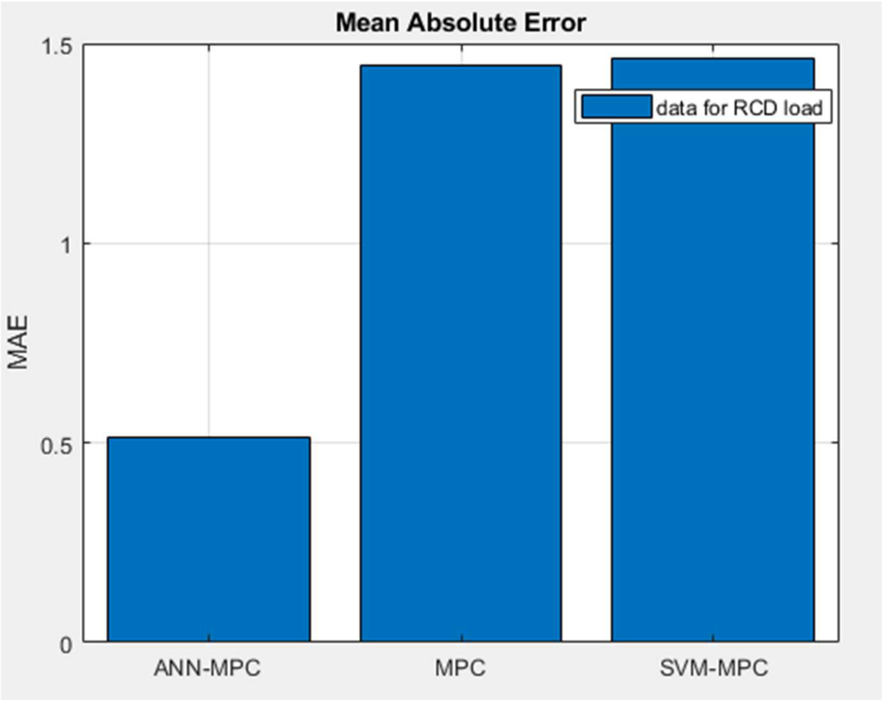

Figure 3.29: Controllers' tracking error for nonlinear loading.

Chapter 4 : Experimental Results

In this section, the controllers simulated will be programmed into the dSPACE MicroLabBox and placed in a three-phase inverter control loop. The inverter will be tested in as the previous chapter. The performance of the inverter was expected to be close to the simulations for each control model.

4.1 Testing overview and set-up

The Simulink models that were created in the previous chapter were programmed into the MicroLabBox to be tested. Computational loading on the MicroLabBox was measured for each control model for comparison purposes. The hardware set-up used during testing is seen in figure 4.1. the load would change depending on the test from resistive to nonlinear.

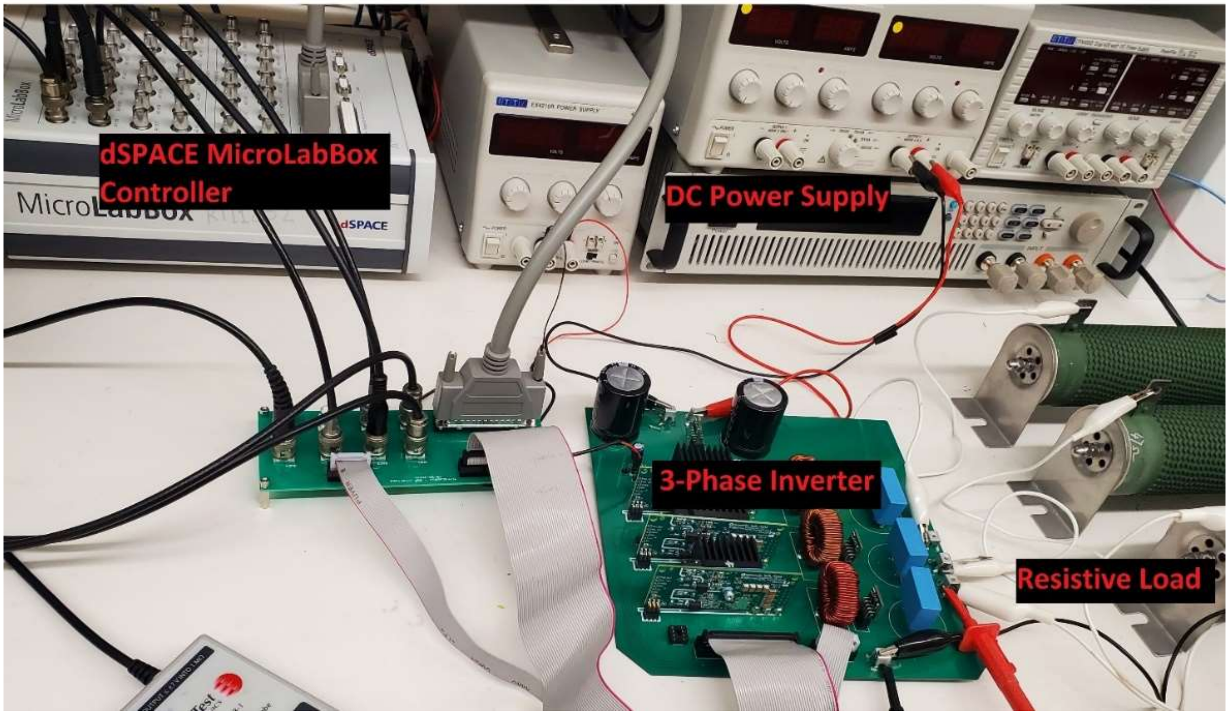

Figure 4.1: Three-phase inverter set-up.

4.2 Testing Scenarios

4.2.1 Static Loads

The first test scenario consisted of capturing the performance of each model under a resistive and nonlinear load. The THD and MAE were calculated for each load type. A resistive load of 47-Ω was used to acquire the training samples for the machine learning models, this will be referred to as the training load. All models were tested under the training load and a 32-Ω resistive load; this tested the machine-learning models' performance at different loads.

Figure 4.2 shows the three-phase voltage output and the ten highest harmonics up to the 13th harmonic while driving a 47-ohm load.

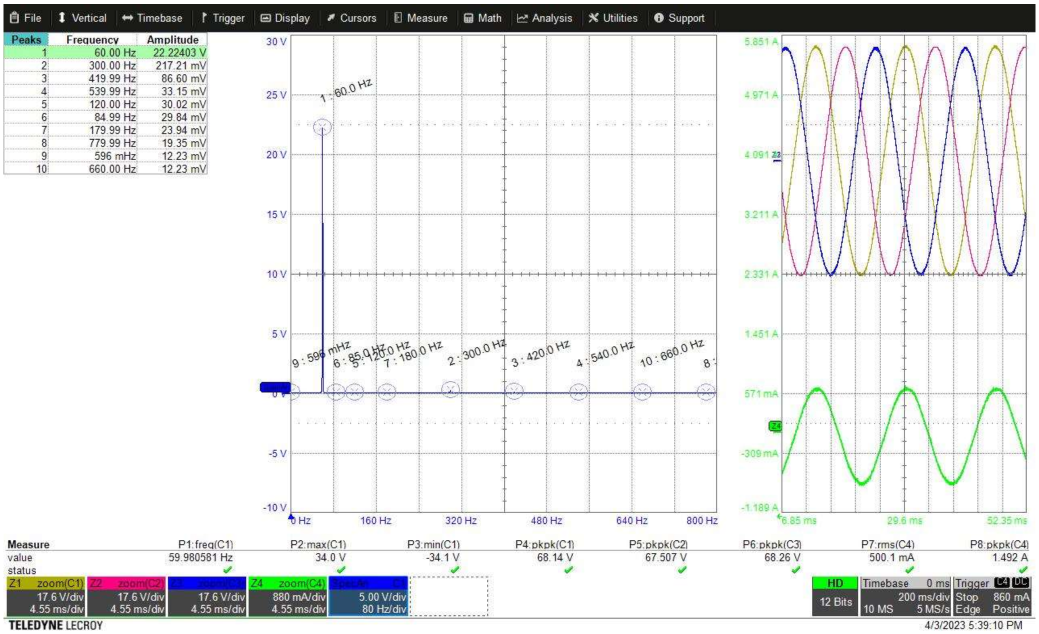

Peaks	Frequency	Amplitude
1	60.00 Hz	22.22403 V
2	300.00 Hz	217.21 mV
3	419.99 Hz	86.60 mV
4	539.99 Hz	33.15 mV
5	120.00 Hz	30.02 mV
6	84.99 Hz	29.84 mV
7	179.99 Hz	23.94 mV
8	779.99 Hz	19.35 mV
9	596 mHz	12.23 mV
10	660.00 Hz	12.23 mV

Measure	P1:freq(C1)	P2:max(C1)	P3:min(C1)	P4:pkpk(C1)	P5:pkpk(C2)	P6:pkpk(C3)	P7:rms(C4)	P8:pkpk(C4)
value	59.980581 Hz	34.0 V	-34.1 V	68.14 V	67.507 V	68.26 V	500.1 mA	1.492 A
status	✓	✓	✓	✓	✓	✓	✓	✓

Z1 zoom(C1)	Z2 zoom(C2)	Z3 zoom(C3)	Z4 zoom(C4)	Spectrum C1
17.6 V/div 4.55 ms/div	17.6 V/div 4.55 ms/div	17.6 V/div 4.55 ms/div	880 mA/div 4.55 ms/div	5.00 V/div 80 Hz/div

HD	Timebase 0 ms	Trigger C4 DC
12 Bits	200 ms/div 10 MS 5 MS/s	Stop 860 mA Edge Positive

4/3/2023 5:39:10 PM

Figure 4.2: MPC’s performance with a 47Ω load

As can be seen in figure 4.2, the MPC performs well with the training load. The tracking error was also captured and shown in figure 4.3. As expected, the MPC can track the reference which results in the three-phase output voltage. These samples were exported and the THD and MAE were calculated for comparison. The values calculated will be compared with the other control models.

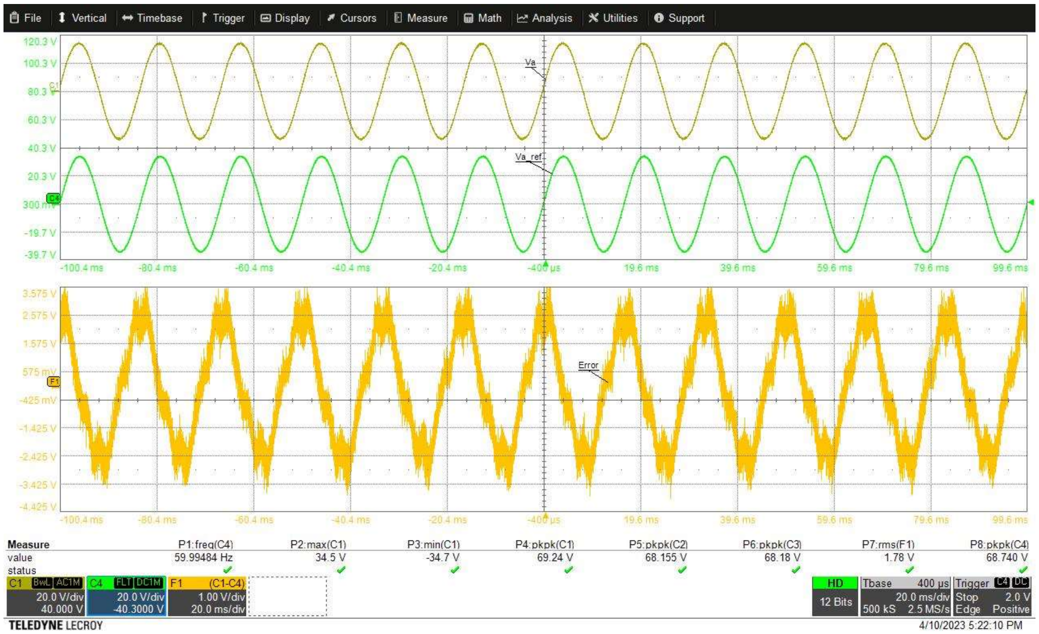

Measure	P1:freq(C4)	P2:max(C1)	P3:min(C1)	P4:pkpk(C1)	P5:pkpk(C2)	P6:pkpk(C3)	P7:rms(F1)	P8:pkpk(C4)
value	59.99484 Hz	34.5 V	-34.7 V	69.24 V	68.155 V	68.18 V	1.78 V	68.740 V
status	✓	✓	✓	✓	✓	✓	✓	✓

C1 BwL AC1M 20.0 V/div 40.000 V
C4 FLT DC1M 20.0 V/div -40.3000 V
F1 (C1-C4) 1.00 V/div 20.0 ms/div
HD 12 Bits
Tbase 400 µs 20.0 ms/div 500 kS 2.5 MS/s
Trigger C4 DC Stop 2.0 V Edge Positive
4/10/2023 5:22:10 PM

Figure 4.3: MPC’s error tracking with a 47-ohm load.

Next, the ANN-MPC model was loaded onto the MicroLabBox, and the procedure was repeated. Figure 4.4 shows the ANN-MPC output the three-phase voltage waveform successfully; the ten highest harmonics can also be seen.

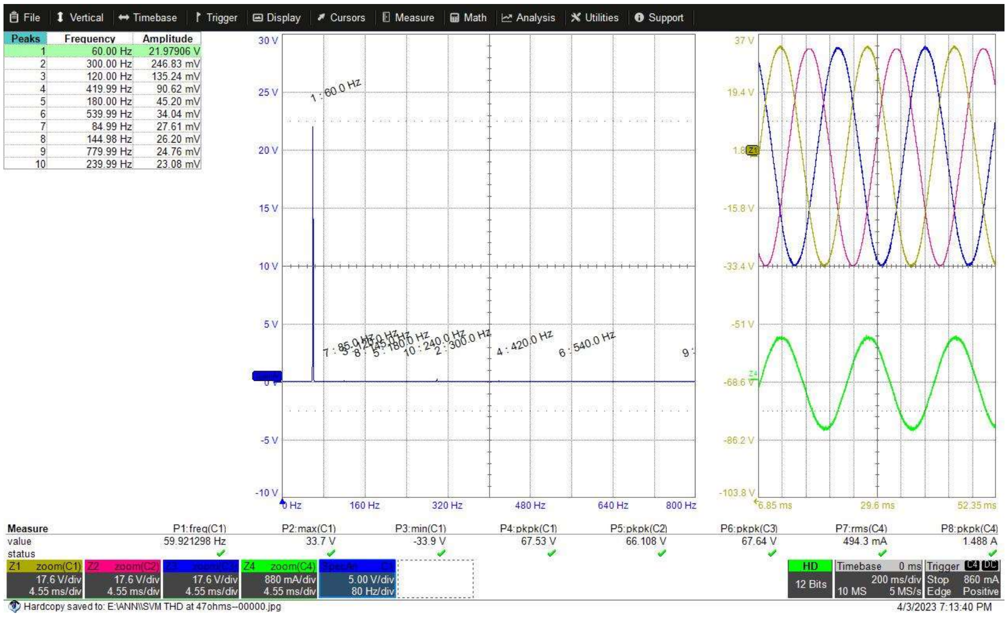

Peaks	Frequency	Amplitude
1	60.00 Hz	21.97906 V
2	300.00 Hz	246.83 mV
3	120.00 Hz	135.24 mV
4	419.99 Hz	90.62 mV
5	180.00 Hz	45.20 mV
6	539.99 Hz	34.04 mV
7	84.99 Hz	27.61 mV
8	144.98 Hz	26.20 mV
9	779.99 Hz	24.76 mV
10	239.99 Hz	23.08 mV

Measure	P1:freq(C1)	P2:max(C1)	P3:min(C1)	P4:pkpk(C1)	P5:pkpk(C2)	P6:pkpk(C3)	P7:rms(C4)	P8:pkpk(C4)
value	59.921298 Hz	33.7 V	-33.9 V	67.53 V	66.108 V	67.64 V	494.3 mA	1.488 A
status	✓	✓	✓	✓	✓	✓	✓	✓

Hardcopy saved to: E:\ANN\\SVM THD at 47ohms--00000.jpg

4/3/2023 7:13:40 PM

Figure 4.4: ANN controller’s performance with a 47ohm load.

The tracking error was obtained from this controller as well and the MAE and THD were calculated for comparison. Figure 4.5 shows the tracking error for the ANN based controller. From the captures taken one can see that the ANN can output a clean waveform just like the MPC. The tracking error can also be seen to be lower than the MPC.

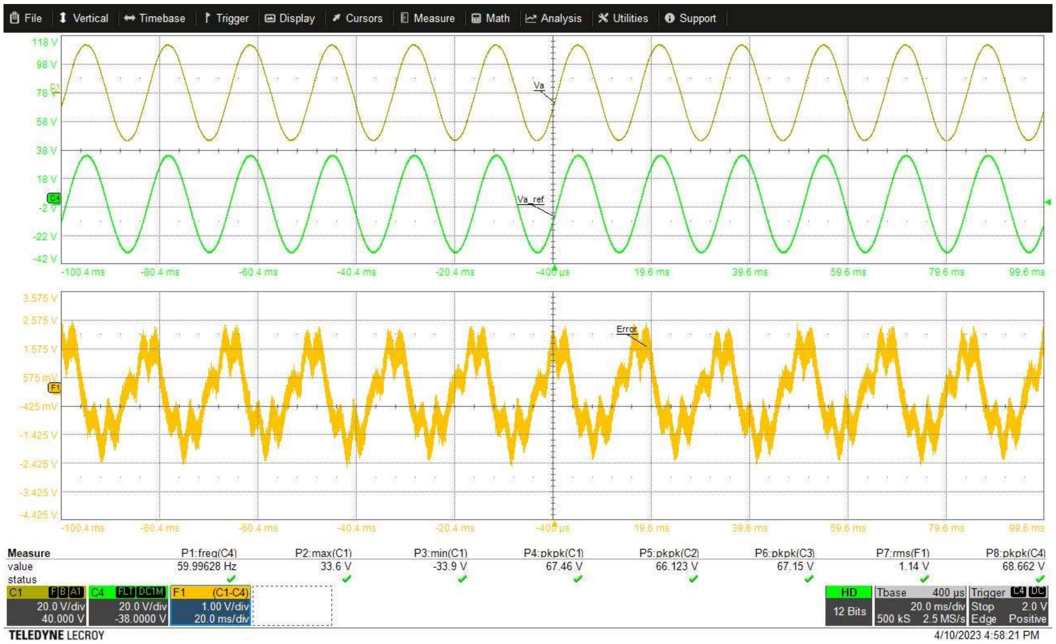

Measure	P1:freq(C4)	P2:max(C1)	P3:min(C1)	P4:pkpk(C1)	P5:pkpk(C2)	P6:pkpk(C3)	P7:rms(F1)	P8:pkpk(C4)
value	59.99628 Hz	33.6 V	-33.9 V	67.46 V	66.123 V	67.15 V	1.14 V	68.662 V
status	✓	✓	✓	✓	✓	✓	✓	✓

Figure 4.5: ANN controller’s error tracking with a 47-ohm load.

Finally, the SVM based controller was tested in the same manner and the performance captured in figures 4.6 and 4.7. As seen in chapter 3, the SVM-MPC can track the error comparably to the MPC and ANN-MPC. In fact, like the ANN, the tracking error is seen to be lower than the MPC.

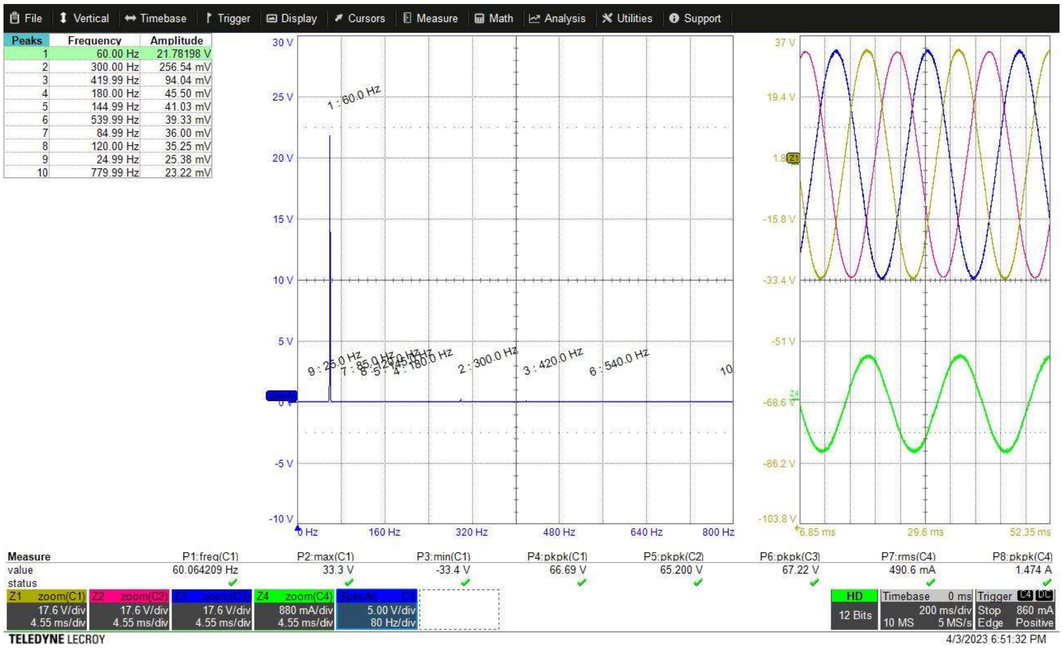

Peaks	Frequency	Amplitude
1	60.00 Hz	21.78198 V
2	300.00 Hz	256.54 mV
3	419.99 Hz	94.04 mV
4	180.00 Hz	45.50 mV
5	144.99 Hz	41.03 mV
6	539.99 Hz	39.33 mV
7	84.99 Hz	36.00 mV
8	120.00 Hz	35.25 mV
9	24.99 Hz	25.38 mV
10	779.99 Hz	23.22 mV

Measure	P1:freq(C1)	P2:max(C1)	P3:min(C1)	P4:pkpk(C1)	P5:pkpk(C2)	P6:pkpk(C3)	P7:rms(C4)	P8:pkpk(C4)
value	60.064209 Hz	33.3 V	-33.4 V	66.69 V	65.200 V	67.22 V	490.6 mA	1.474 A
status	✓	✓	✓	✓	✓	✓	✓	✓

Z1 zoom(C1)	Z2 zoom(C2)	Z3 zoom(C3)	Z4 zoom(C4)	Spectrum C1
17.6 V/div	17.6 V/div	17.6 V/div	880 mA/div	5.00 V/div
4.55 ms/div	4.55 ms/div	4.55 ms/div	4.55 ms/div	80 Hz/div

HD 12 Bits
Timebase 0 ms 200 ms/div 10 MS 5 MS/s
Trigger C4 DC Stop 860 mA Edge Positive

4/3/2023 6:51:32 PM

Figure 4.6: SVM-MPC’s performance at 47-ohm.

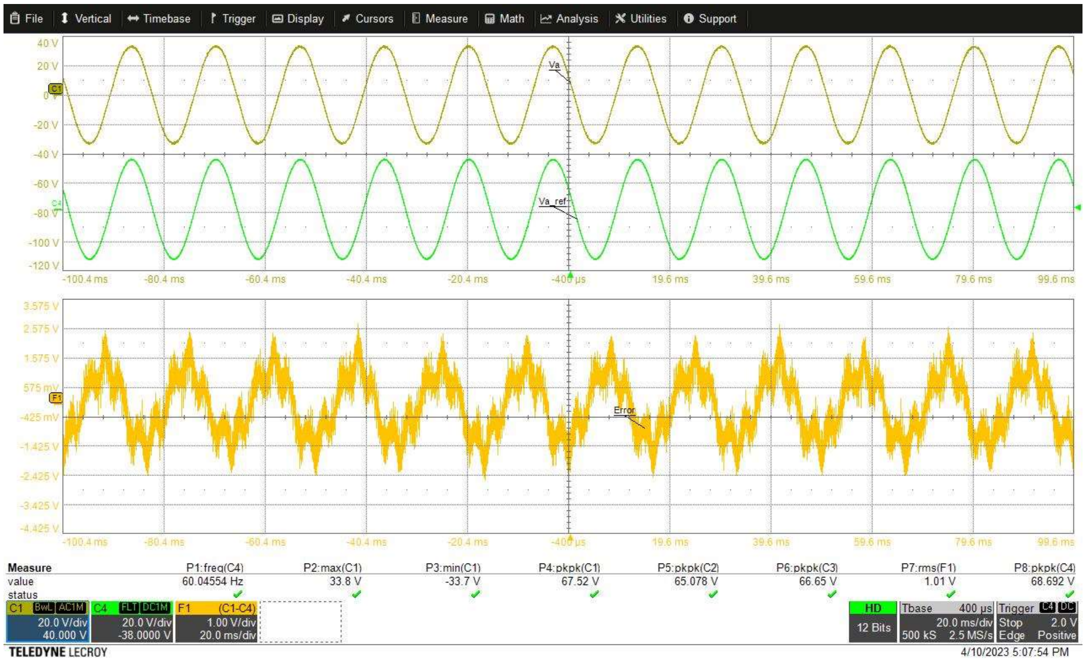

Measure	P1:freq(C4)	P2:max(C1)	P3:min(C1)	P4:pkpk(C1)	P5:pkpk(C2)	P6:pkpk(C3)	P7:rms(F1)	P8:pkpk(C4)
value	60.04554 Hz	33.8 V	-33.7 V	67.52 V	65.078 V	66.65 V	1.01 V	68.692 V
status	✓	✓	✓	✓	✓	✓	✓	✓

C1 BwL AC1M	C4 FLT DC1M	F1 (C1-C4)
20.0 V/div	20.0 V/div	1.00 V/div
40.000 V	-38.0000 V	20.0 ms/div

HD 12 Bits
Tbase 400 µs 20.0 ms/div 500 kS 2.5 MS/s
Trigger C4 DC Stop 2.0 V Edge Positive

4/10/2023 5:07:54 PM

Figure 4.7: SVM error tracking with 47-ohms.

Next, the load was changed to a static 32-ohm load to observe performance at different load conditions than what the machine-learning based controls were trained at. The controls' performance was recorded, and metrics were calculated. An oscilloscope capture showing the MPC's performance and harmonics of 60 Hz can be seen in figure 4.8 along with the tracking error in figure 4.9. From the figures, one can see that the MPC can continue to track the reference albeit with lower amplitude in the fundamental frequency.

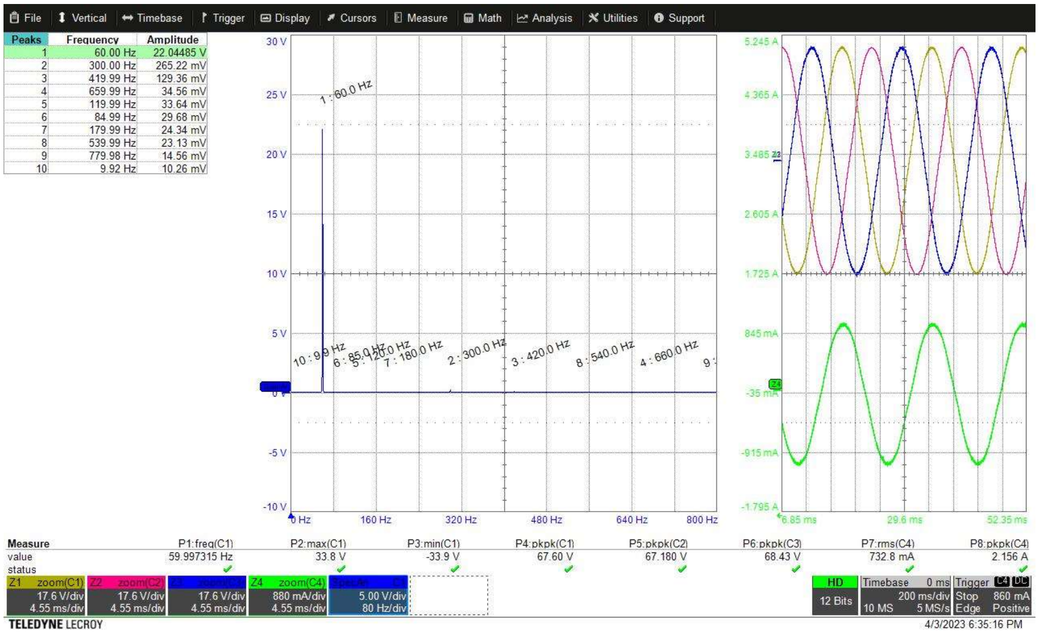

Peaks	Frequency	Amplitude
1	60.00 Hz	22.04485 V
2	300.00 Hz	265.22 mV
3	419.99 Hz	129.36 mV
4	659.99 Hz	34.56 mV
5	119.99 Hz	33.64 mV
6	84.99 Hz	29.68 mV
7	179.99 Hz	24.34 mV
8	539.99 Hz	23.13 mV
9	779.98 Hz	14.56 mV
10	9.92 Hz	10.26 mV

Measure	P1:freq(C1)	P2:max(C1)	P3:min(C1)	P4:pkpk(C1)	P5:pkpk(C2)	P6:pkpk(C3)	P7:rms(C4)	P8:pkpk(C4)
value	59.997315 Hz	33.8 V	-33.9 V	67.60 V	67.180 V	68.43 V	732.8 mA	2.156 A
status	✓	✓	✓	✓	✓	✓	✓	✓

Z1 zoom(C1)	Z2 zoom(C2)	Z3 zoom(C3)	Z4 zoom(C4)	Spectrum C1	HD	Timebase 0 ms	Trigger C4 DC
17.6 V/div 4.55 ms/div	17.6 V/div 4.55 ms/div	17.6 V/div 4.55 ms/div	880 mA/div 4.55 ms/div	5.00 V/div 80 Hz/div	12 Bits	200 ms/div 10 MS 5 MS/s	Stop 860 mA Edge Positive

4/3/2023 6:35:16 PM

Figure 4.8: MPC's performance with a 32-ohm load.

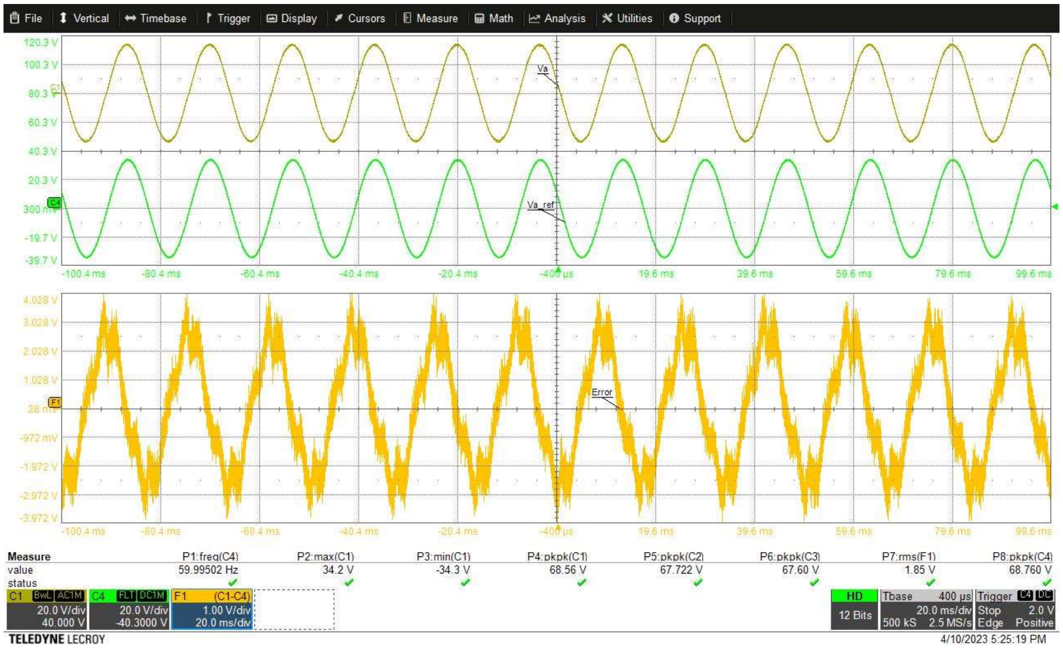

Measure	P1:freq(C4)	P2:max(C1)	P3:min(C1)	P4:pkpk(C1)	P5:pkpk(C2)	P6:pkpk(C3)	P7:rms(F1)	P8:pkpk(C4)
value	59.99502 Hz	34.2 V	-34.3 V	68.56 V	67.722 V	67.60 V	1.85 V	68.760 V
status	✓	✓	✓	✓	✓	✓	✓	✓

C1 BwL AC1M 20.0 V/div 40.000 V

C4 FLT DC1M 20.0 V/div -40.3000 V

F1 (C1-C4) 1.00 V/div 20.0 ms/div

HD 12 Bits

Tbase 400 µs 20.0 ms/div 500 kS 2.5 MS/s

Trigger C4 DC Stop 2.0 V Edge Positive

4/10/2023 5:25:19 PM

Figure 4.9: MPC's error tracking with a 32-ohm load.

The ANN-MPC's performance was then captured as seen in figure 4.10. The fundamental frequency also shows a decrease in amplitude like the MPC which implies a higher THD. Interestingly, the tracking error shown in figure 4.11 is lower for the ANN-MPC than that of the MPC like in the 47-Ohm case. This demonstrates a greater generality on the ANN based controller than the MPC when the load and other parameters change on the plant model.

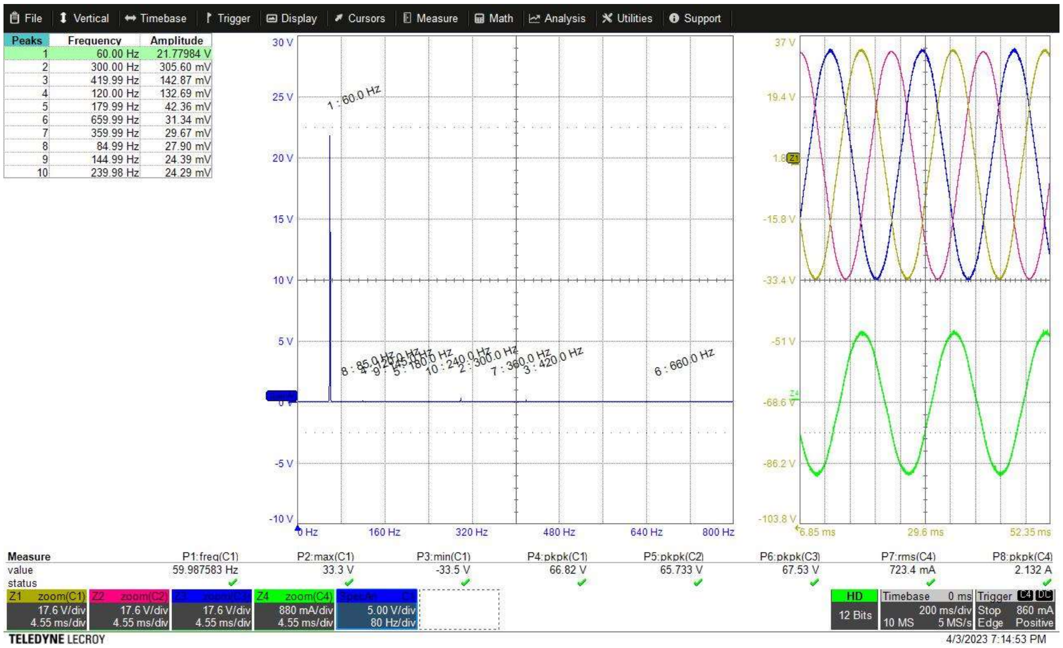

Peaks	Frequency	Amplitude
1	60.00 Hz	21.77984 V
2	300.00 Hz	305.60 mV
3	419.99 Hz	142.87 mV
4	120.00 Hz	132.69 mV
5	179.99 Hz	42.36 mV
6	659.99 Hz	31.34 mV
7	359.99 Hz	29.67 mV
8	84.99 Hz	27.90 mV
9	144.99 Hz	24.39 mV
10	239.98 Hz	24.29 mV

Measure	P1:freq(C1)	P2:max(C1)	P3:min(C1)	P4:pkpk(C1)	P5:pkpk(C2)	P6:pkpk(C3)	P7:rms(C4)	P8:pkpk(C4)
value	59.987583 Hz	33.3 V	-33.5 V	66.82 V	65.733 V	67.53 V	723.4 mA	2.132 A
status	✓	✓	✓	✓	✓	✓	✓	✓

Figure 4.10: ANN-MPC performance with a 32-ohm load.

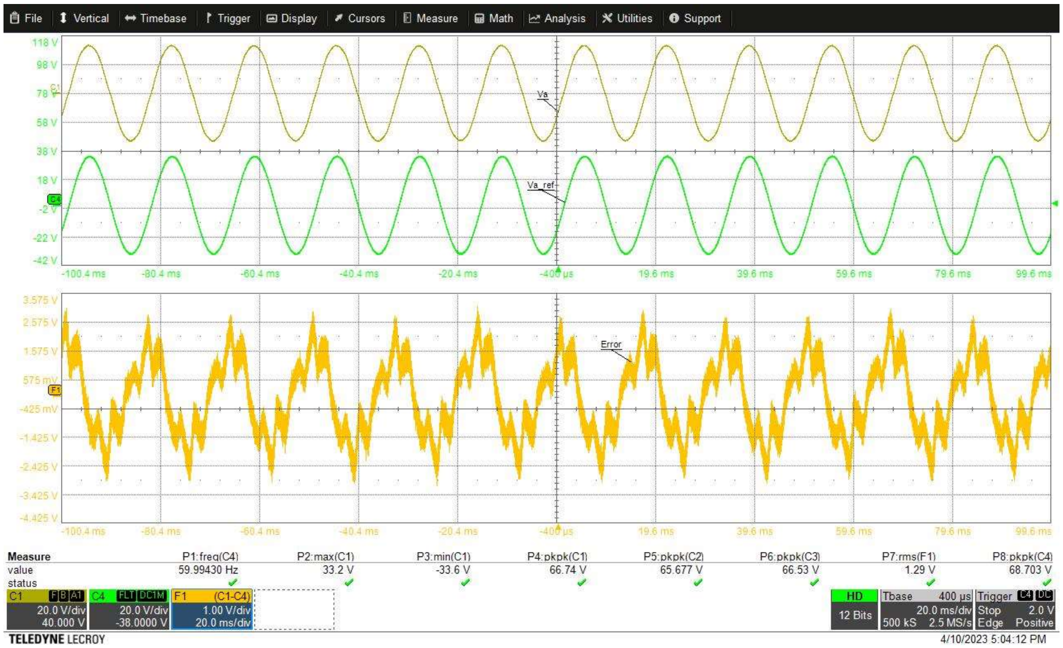

Measure	P1:freq(C4)	P2:max(C1)	P3:min(C1)	P4:pkpk(C1)	P5:pkpk(C2)	P6:pkpk(C3)	P7:rms(F1)	P8:pkpk(C4)
value	59.99430 Hz	33.2 V	-33.6 V	66.74 V	65.677 V	66.53 V	1.29 V	68.703 V
status	✓	✓	✓	✓	✓	✓	✓	✓

Figure 4.11: ANN control error tracking with a 32-ohm load.

Lastly, the SVM-MPC's performance and error can be seen in figures 4.12 and 4.13 respectively. As with the two other models, the THD is higher when not implemented on the training load. The error is also higher for the 32-Ohm case, but it is still lower than the other models. As with the ANN-MPC case, the lower tracking error may be attributed to a faster actuation time. In other words, since the ML-based models are expected to lower computation time due to the offline optimization, they're able to exert the control effort faster and thus tracking the reference better.

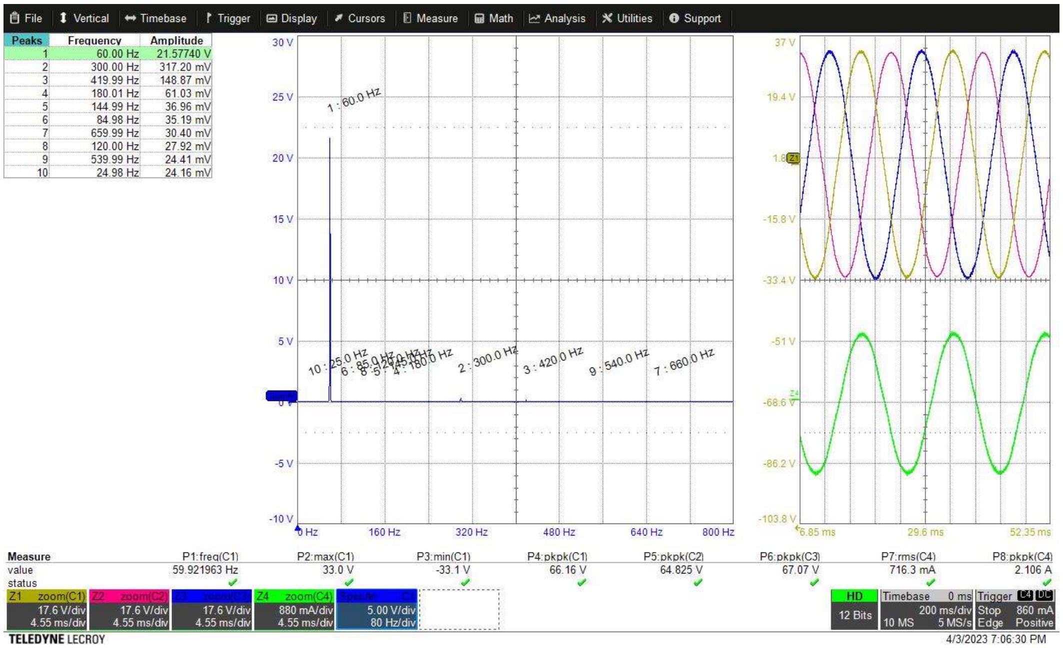

Peaks	Frequency	Amplitude
1	60.00 Hz	21.57740 V
2	300.00 Hz	317.20 mV
3	419.99 Hz	148.87 mV
4	180.01 Hz	61.03 mV
5	144.99 Hz	36.96 mV
6	84.98 Hz	35.19 mV
7	659.99 Hz	30.40 mV
8	120.00 Hz	27.92 mV
9	539.99 Hz	24.41 mV
10	24.98 Hz	24.16 mV

Measure	P1:freq(C1)	P2:max(C1)	P3:min(C1)	P4:pkpk(C1)	P5:pkpk(C2)	P6:pkpk(C3)	P7:rms(C4)	P8:pkpk(C4)
value	59.921963 Hz	33.0 V	-33.1 V	66.16 V	64.825 V	67.07 V	716.3 mA	2.106 A
status	✓	✓	✓	✓	✓	✓	✓	✓

Z1 zoom(C1)	Z2 zoom(C2)	Z3 zoom(C3)	Z4 zoom(C4)	Spectrum C1
17.6 V/div 4.55 ms/div	17.6 V/div 4.55 ms/div	17.6 V/div 4.55 ms/div	880 mA/div 4.55 ms/div	5.00 V/div 80 Hz/div

HD 12 Bits

Timebase 0 ms 200 ms/div 10 MS 5 MS/s

Trigger C4 DC Stop 860 mA Edge Positive

4/3/2023 7:06:30 PM

Figure 4.12: SVM-MPC performance with a 32-ohm load.

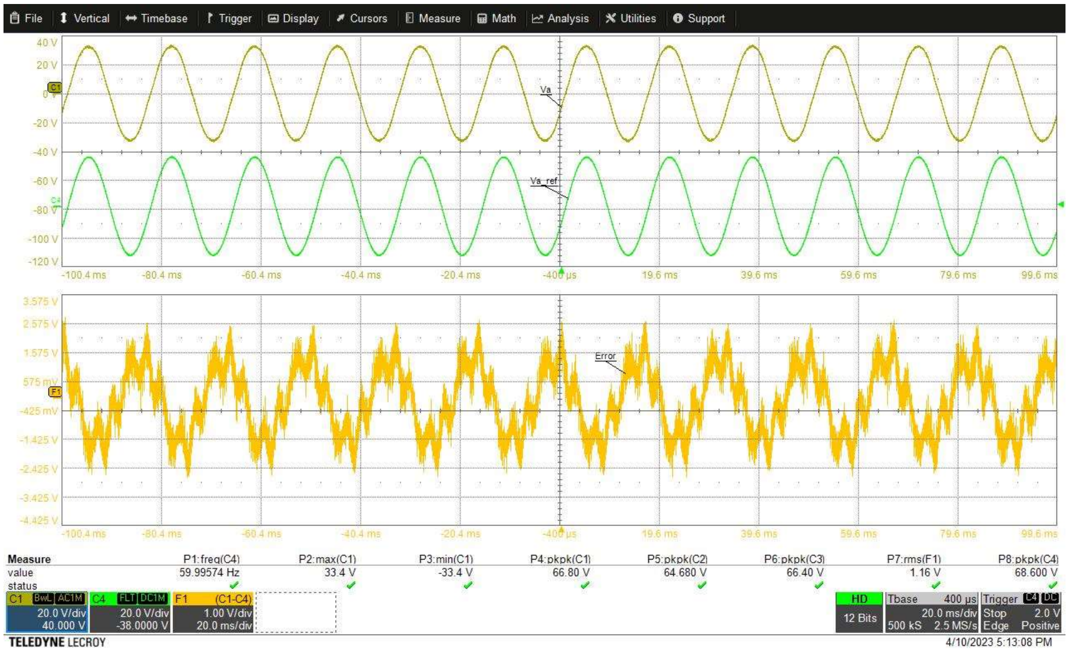

Measure	P1:freq(C4)	P2:max(C1)	P3:min(C1)	P4:pkpk(C1)	P5:pkpk(C2)	P6:pkpk(C3)	P7:rms(F1)	P8:pkpk(C4)
value	59.99574 Hz	33.4 V	-33.4 V	66.80 V	64.680 V	66.40 V	1.16 V	68.600 V
status	✓	✓	✓	✓	✓	✓	✓	✓

C1 BwL AC1M 20.0 V/div 40.000 V
C4 FLT DC1M 20.0 V/div -38.0000 V
F1 (C1-C4) 1.00 V/div 20.0 ms/div
HD 12 Bits
Tbase 400 µs 20.0 ms/div 500 kS 2.5 MS/s
Trigger C4 DC Stop 2.0 V Edge Positive
4/10/2023 5:13:08 PM

Figure 4.13: SVM-MPC error tracking with a 32-ohm load.

The quantities obtained from the experiments above are compiled in figures 4.14 and 4.15 for comparison. As can be seen from the figures, the three controllers had similar performance, but the reference tracking is better for the ML-based control models. The computation time for each controller is explored in a later section. The THD is expected to be higher for the ML-based controllers since these are trained using MPC samples.

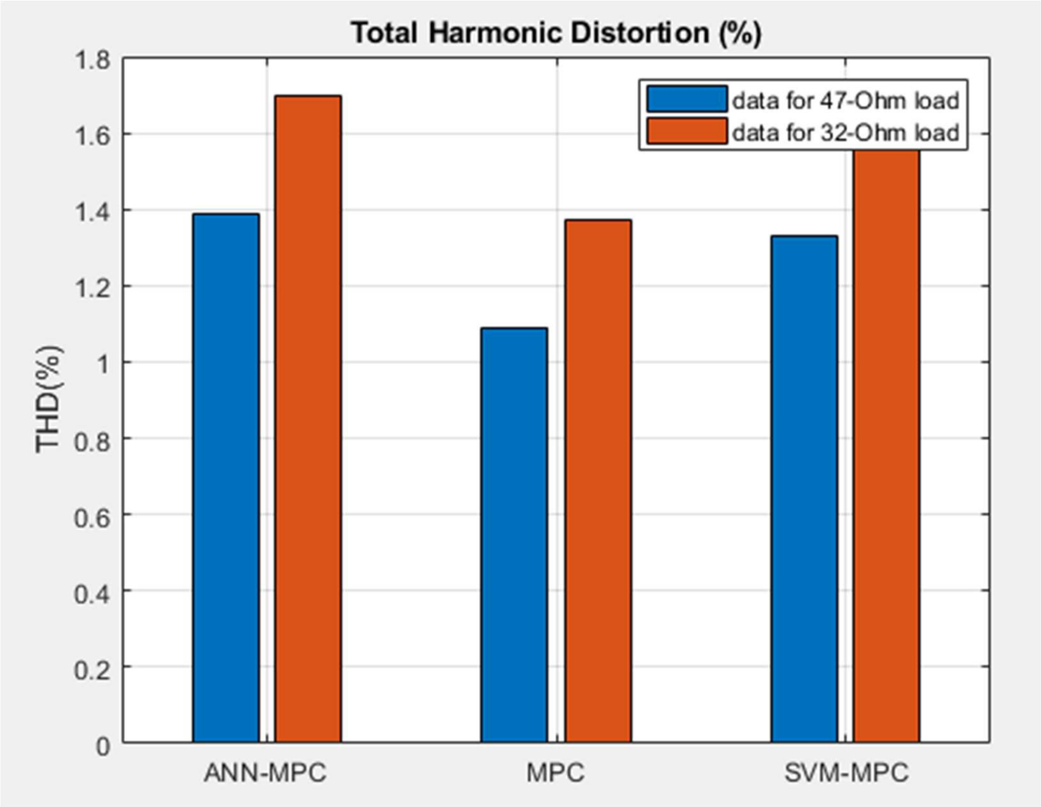

Figure 4.14 Control THD at different resistive loads.

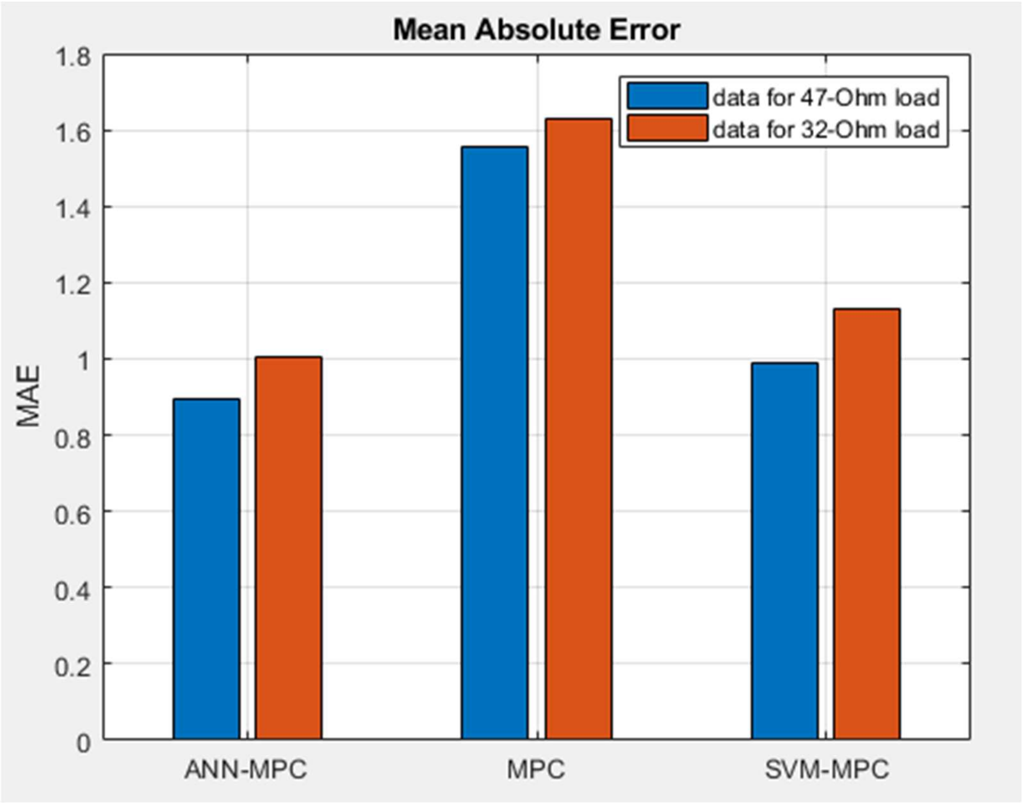

Figure 4.15 Control MAE at different resistive loads.

Further comparison will be seen at the end of this chapter including the data from all the other tests.

4.2.2 Dynamic load test

The next test set involved changing the load and recording the controls' performance during the change. Ideally, the control being tested should maintain the voltage as close as possible to the reference. During the change in load there should be a clear change in current to reflect the load. Figure 4.16 shows the inverter's voltage being controlled by the MPC during the load change.

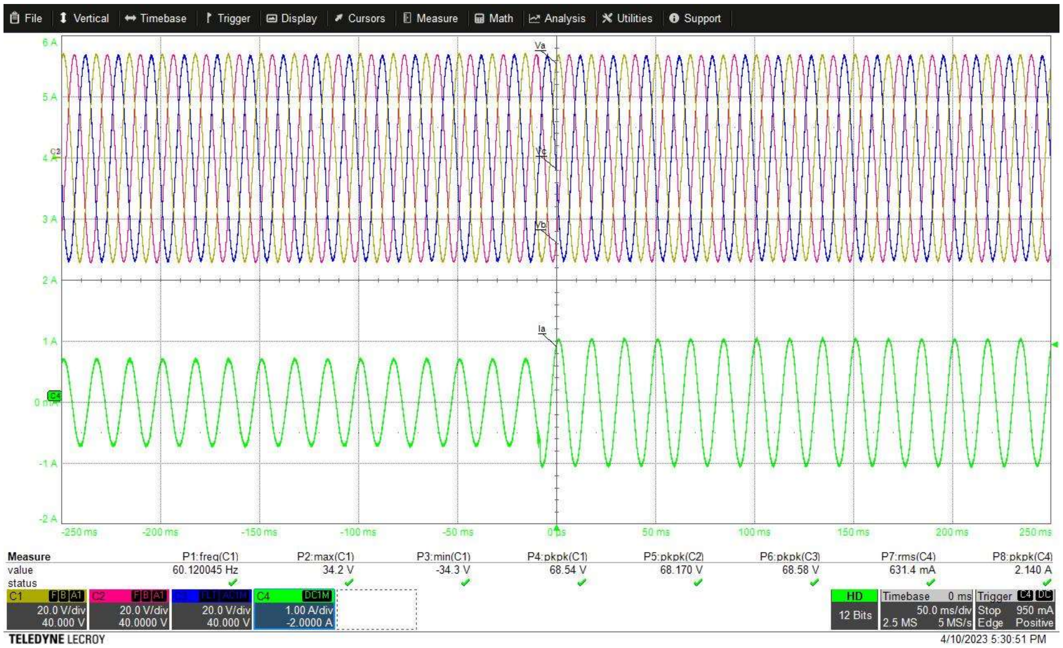

Measure	P1:freq(C1)	P2:max(C1)	P3:min(C1)	P4:pkpk(C1)	P5:pkpk(C2)	P6:pkpk(C3)	P7:rms(C4)	P8:pkpk(C4)
value	60.120045 Hz	34.2 V	-34.3 V	68.54 V	68.170 V	68.58 V	631.4 mA	2.140 A
status	✓	✓	✓	✓	✓	✓	✓	✓

C1	C2	C3	C4 DC1M
20.0 V/div	20.0 V/div	20.0 V/div	1.00 A/div
40.000 V	40.0000 V	40.000 V	-2.0000 A

HD 12 Bits
Timebase 0 ms 50.0 ms/div 2.5 MS 5 MS/s
Trigger C4 DC Stop 950 mA Edge Positive
4/10/2023 5:30:51 PM

Figure 4.16: MPC performance during load change.

As expected, the current increases when the load changes from 47-Ohms to 32-Ohms but the voltage remains at its intended value.

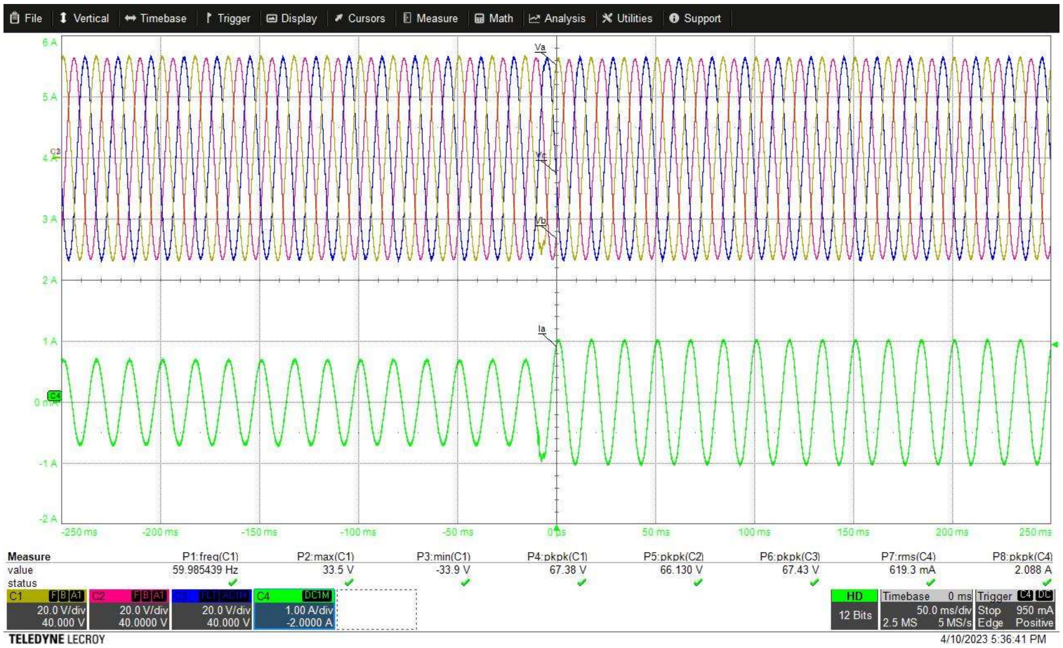

Measure	P1:freq(C1)	P2:max(C1)	P3:min(C1)	P4:pkpk(C1)	P5:pkpk(C2)	P6:pkpk(C3)	P7:rms(C4)	P8:pkpk(C4)
value	59.985439 Hz	33.5 V	-33.9 V	67.38 V	66.130 V	67.43 V	619.3 mA	2.088 A
status	✓	✓	✓	✓	✓	✓	✓	✓

C1 F B A1 20.0 V/div 40.000 V

C2 F B A1 20.0 V/div 40.0000 V

20.0 V/div 40.000 V

C4 DC1M 1.00 A/div -2.0000 A

HD 12 Bits

Timebase 0 ms 50.0 ms/div 2.5 MS 5 MS/s

Trigger C4 DC Stop 950 mA Edge Positive

4/10/2023 5:36:41 PM

Figure 4.17: ANN-MPC control performance during load change

Figure 4.17 shows the ANN based controller during the same test. The control performed similarly to the MPC. To finish this test, the SVM based controller was tested and recorded as shown in figure 4.18.

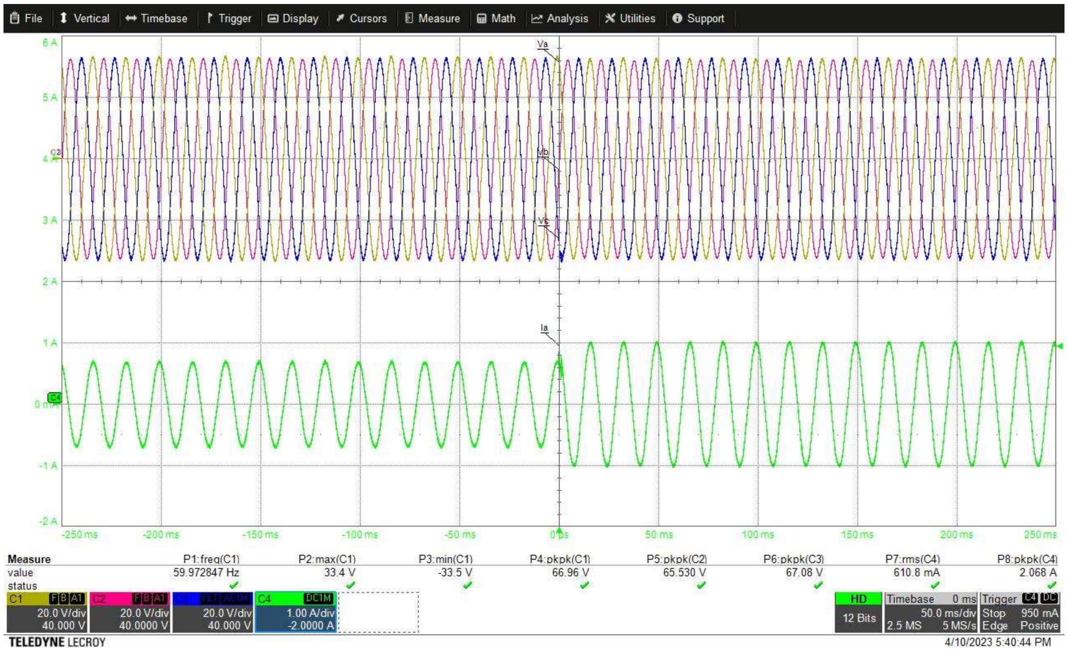

Measure	P1:freq(C1)	P2:max(C1)	P3:min(C1)	P4:pkpk(C1)	P5:pkpk(C2)	P6:pkpk(C3)	P7:rms(C4)	P8:pkpk(C4)
value	59.972847 Hz	33.4 V	-33.5 V	66.96 V	65.530 V	67.08 V	610.8 mA	2.068 A
status	✓	✓	✓	✓	✓	✓	✓	✓

C1 F B A1	C2 F B A1	C3	C4 DC1M
20.0 V/div 40.000 V	20.0 V/div 40.0000 V	20.0 V/div 40.000 V	1.00 A/div -2.0000 A

HD	Timebase 0 ms	Trigger C4 DC
12 Bits	50.0 ms/div 2.5 MS 5 MS/s	Stop 950 mA Edge Positive

4/10/2023 5:40:44 PM

Figure 4.18: SVM-MPC control performance during load change.

In conclusion, the controls remained stable during the load change and there was minimal change to the voltage during the switch. Since all models showed similar performance, this hints to a fast response time when faced with sudden changes. This was expected for the MPC since this is one of its features. The ML-based controls demonstrated the same performance which was a sign that they inherited these important features from the MPC.

4.2.3 Nonlinear loading

Modern loads like consumer electronics draw nonlinear current, it’s important for the inverter’s voltage to maintain stability during these situations. Testing the controllers using a nonlinear load will show their performance in terms of voltage THD. The inverter must remain under the stated five percent THD for this test despite the non-linear load.

To continue the sequence of testing used in previous sections, the MPC model was tested using the set-up shown in figure 4.19 which is equivalent to the model in chapter 3 consisting of a three-phase rectifier.

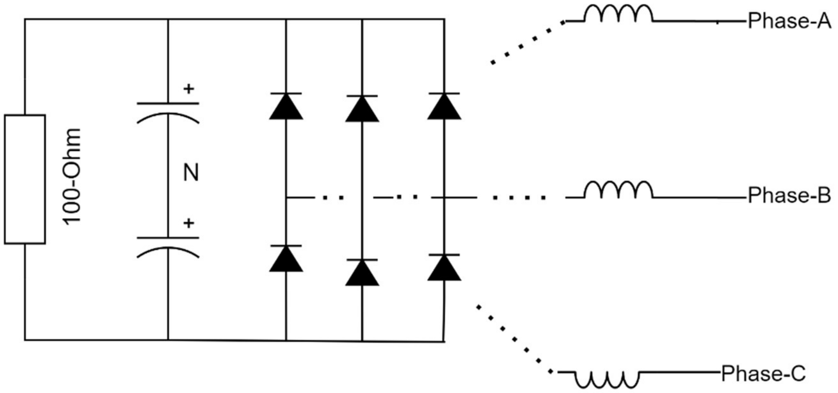

Figure 4.19: Nonlinear load experimental set-up.

The scope capture showing the harmonic magnitude for the MPC nonlinear load test is shown in figure 4.20. These magnitudes will be used to calculate THD and compared to the other controller models.

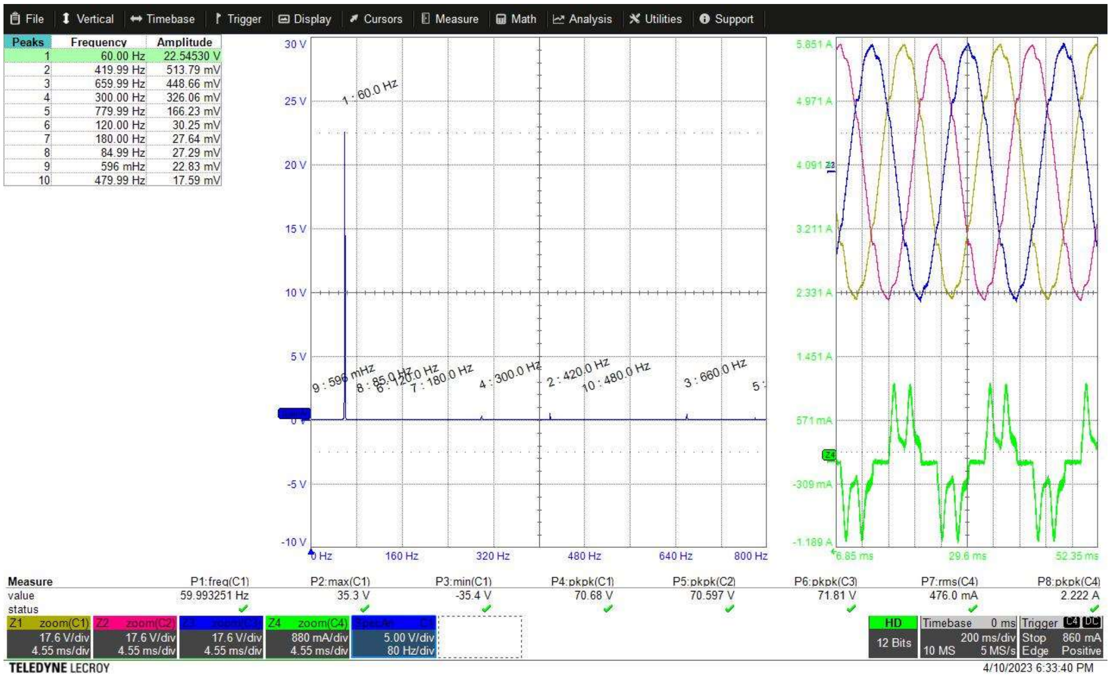

Peaks	Frequency	Amplitude
1	60.00 Hz	22.54530 V
2	419.99 Hz	513.79 mV
3	659.99 Hz	448.66 mV
4	300.00 Hz	326.06 mV
5	779.99 Hz	166.23 mV
6	120.00 Hz	30.25 mV
7	180.00 Hz	27.64 mV
8	84.99 Hz	27.29 mV
9	596 mHz	22.83 mV
10	479.99 Hz	17.59 mV

Measure	P1:freq(C1)	P2:max(C1)	P3:min(C1)	P4:pkpk(C1)	P5:pkpk(C2)	P6:pkpk(C3)	P7:rms(C4)	P8:pkpk(C4)
value	59.993251 Hz	35.3 V	-35.4 V	70.68 V	70.597 V	71.81 V	476.0 mA	2.222 A
status	✓	✓	✓	✓	✓	✓	✓	✓

Z1 zoom(C1)	Z2 zoom(C2)	Z3 zoom(C3)	Z4 zoom(C4)	SpecAn C1
17.6 V/div 4.55 ms/div	17.6 V/div 4.55 ms/div	17.6 V/div 4.55 ms/div	880 mA/div 4.55 ms/div	5.00 V/div 80 Hz/div

HD 12 Bits | Timebase 0 ms 200 ms/div 10 MS 5 MS/s | Trigger C4 DC Stop 860 mA Edge Positive

4/10/2023 6:33:40 PM

Figure 4.20: MPC performance with a nonlinear load.

The control’s ability to track the error between measured value and the reference assigned is also an important measure to compare. Figure 4.21 shows this error tracking for the MPC’s voltage output with a nonlinear load for a single phase. This quantity will be compared with the data from the other models.

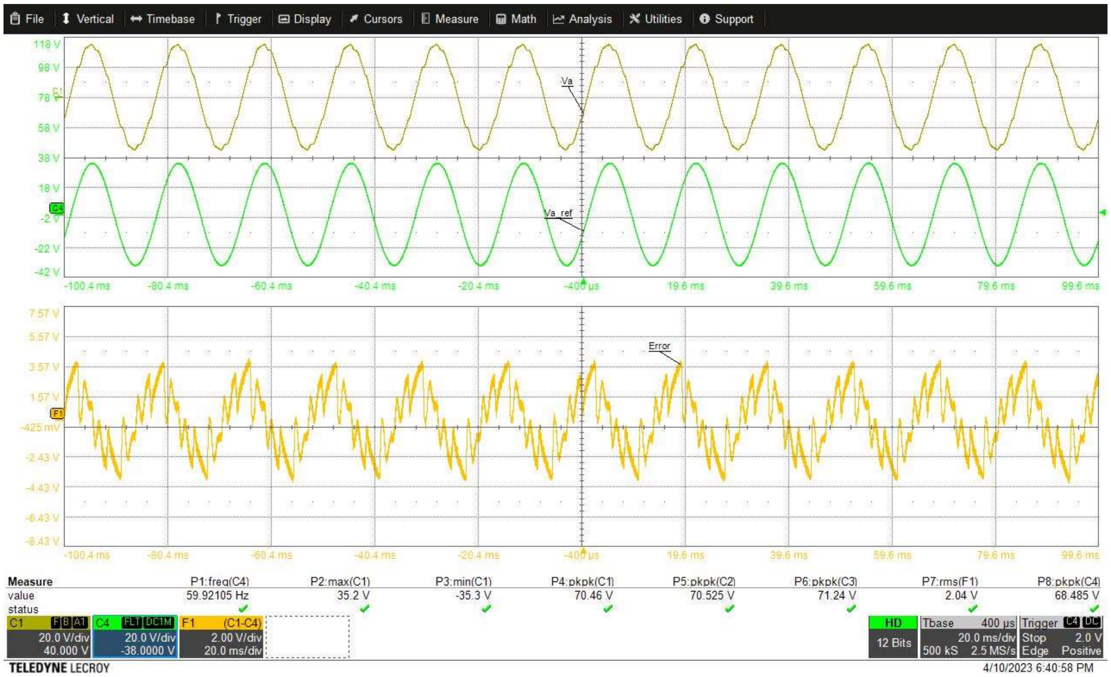

Measure	P1:freq(C4)	P2:max(C1)	P3:min(C1)	P4:pkpk(C1)	P5:pkpk(C2)	P6:pkpk(C3)	P7:rms(F1)	P8:pkpk(C4)
value	59.92105 Hz	35.2 V	-35.3 V	70.46 V	70.525 V	71.24 V	2.04 V	68.485 V
status	✓	✓	✓	✓	✓	✓	✓	✓

Figure 4.21: MPC error tracking with a nonlinear load.

The experiment was repeated for the ANN-MPC model, and the harmonic and error magnitudes was collected as seen in figure 4.22 and figure 4.23. It’s important to note that the error is expected to be higher than for a purely resistive load due to the notching caused by the rectifier commutations.

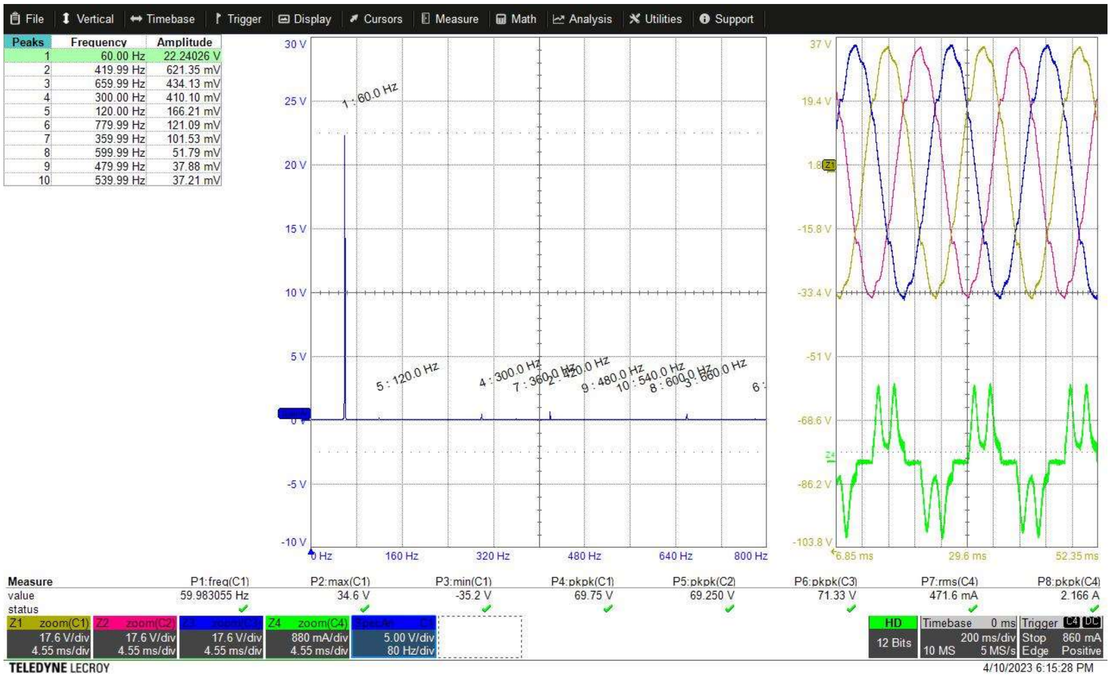

Peaks	Frequency	Amplitude
1	60.00 Hz	22.24026 V
2	419.99 Hz	621.35 mV
3	659.99 Hz	434.13 mV
4	300.00 Hz	410.10 mV
5	120.00 Hz	166.21 mV
6	779.99 Hz	121.09 mV
7	359.99 Hz	101.53 mV
8	599.99 Hz	51.79 mV
9	479.99 Hz	37.88 mV
10	539.99 Hz	37.21 mV

Measure	P1:freq(C1)	P2:max(C1)	P3:min(C1)	P4:pkpk(C1)	P5:pkpk(C2)	P6:pkpk(C3)	P7:rms(C4)	P8:pkpk(C4)
value	59.983055 Hz	34.6 V	-35.2 V	69.75 V	69.250 V	71.33 V	471.6 mA	2.166 A
status	✓	✓	✓	✓	✓	✓	✓	✓

Z1 zoom(C1)	Z2 zoom(C2)	Z3 zoom(C3)	Z4 zoom(C4)	Spectr C1
17.6 V/div	17.6 V/div	17.6 V/div	880 mA/div	5.00 V/div
4.55 ms/div	4.55 ms/div	4.55 ms/div	4.55 ms/div	80 Hz/div

HD 12 Bits
Timebase 0 ms 200 ms/div 10 MS 5 MS/s
Trigger C4 DC Stop 860 mA Edge Positive
4/10/2023 6:15:28 PM

Figure 4.22: ANN-MPC control performance with a nonlinear load.

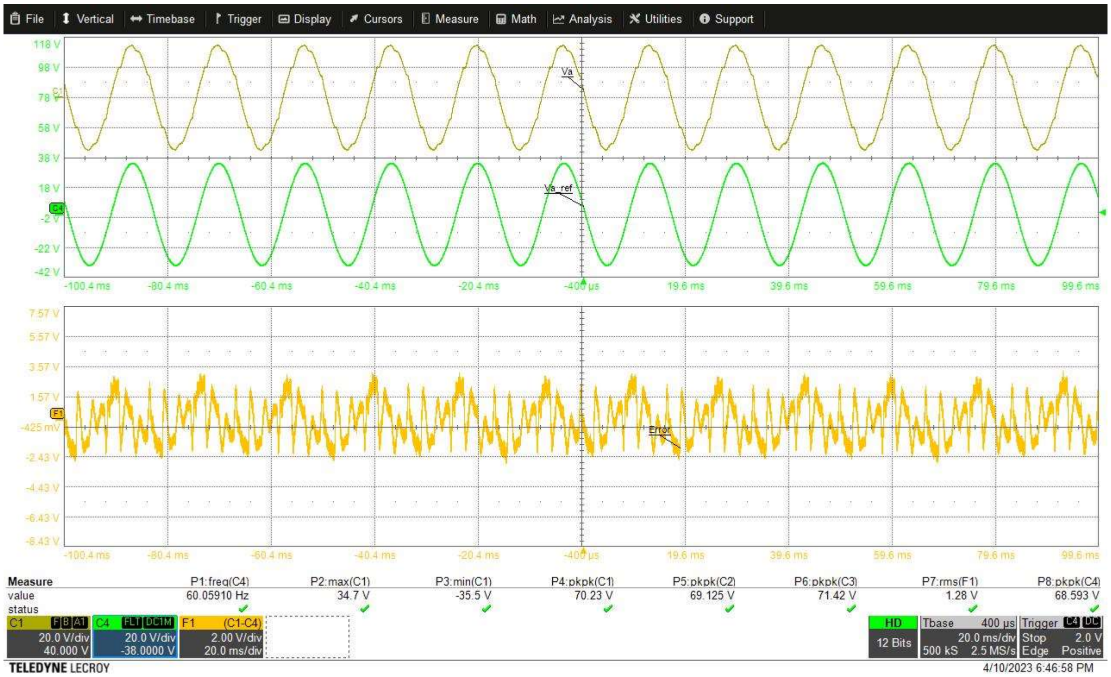

Measure	P1:freq(C4)	P2:max(C1)	P3:min(C1)	P4:pkpk(C1)	P5:pkpk(C2)	P6:pkpk(C3)	P7:rms(F1)	P8:pkpk(C4)
value	60.05910 Hz	34.7 V	-35.5 V	70.23 V	69.125 V	71.42 V	1.28 V	68.593 V
status	✓	✓	✓	✓	✓	✓	✓	✓

C1 F B A1	C4 FLT DC1M	F1 (C1-C4)
20.0 V/div	20.0 V/div	2.00 V/div
40.000 V	-38.0000 V	20.0 ms/div

HD 12 Bits
Tbase 400 µs 20.0 ms/div 500 kS 2.5 MS/s
Trigger C4 DC Stop 2.0 V Edge Positive
4/10/2023 6:46:58 PM

Figure 4.23: ANN-MPC reference tracking error with a nonlinear load.

Similarly, the SVM-MPC model was tested, and scope captures and data were collected for analysis and comparison. This can be seen in figure 4.24 and figure 4.25.

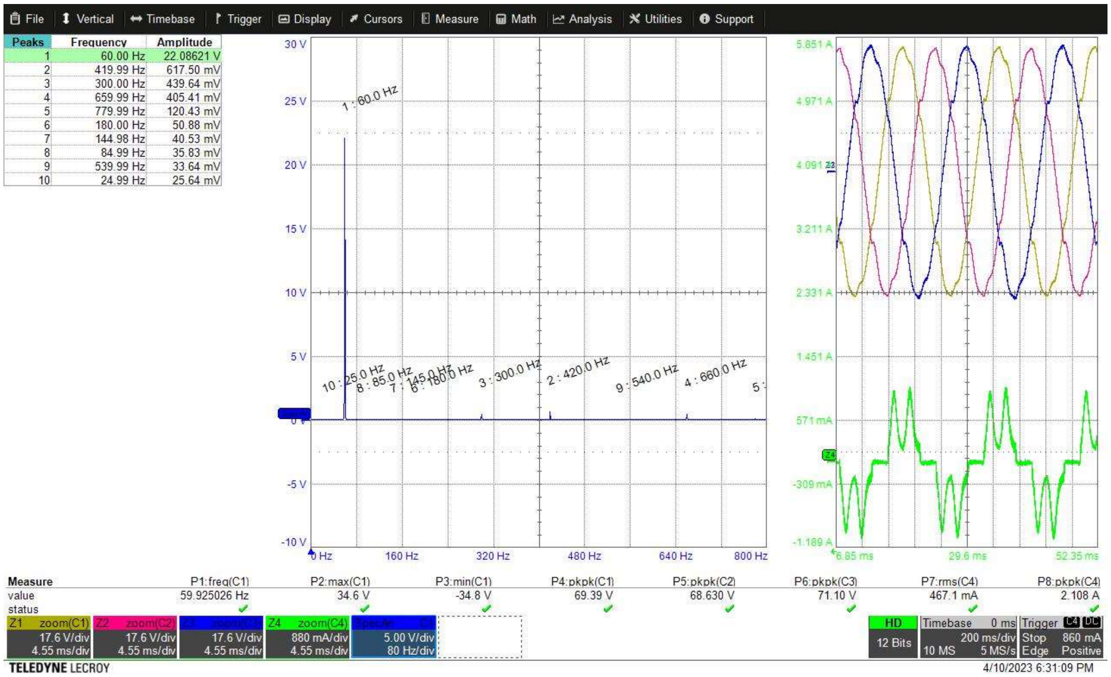

Peaks	Frequency	Amplitude
1	60.00 Hz	22.08621 V
2	419.99 Hz	617.50 mV
3	300.00 Hz	439.64 mV
4	659.99 Hz	405.41 mV
5	779.99 Hz	120.43 mV
6	180.00 Hz	50.88 mV
7	144.98 Hz	40.53 mV
8	84.99 Hz	35.83 mV
9	539.99 Hz	33.64 mV
10	24.99 Hz	25.64 mV

Measure	P1:freq(C1)	P2:max(C1)	P3:min(C1)	P4:pkpk(C1)	P5:pkpk(C2)	P6:pkpk(C3)	P7:rms(C4)	P8:pkpk(C4)
value	59.925026 Hz	34.6 V	-34.8 V	69.39 V	68.630 V	71.10 V	467.1 mA	2.108 A
status	✓	✓	✓	✓	✓	✓	✓	✓

Z1 zoom(C1)	Z2 zoom(C2)	Z3 zoom(C3)	Z4 zoom(C4)	Spectrum C1
17.6 V/div 4.55 ms/div	17.6 V/div 4.55 ms/div	17.6 V/div 4.55 ms/div	880 mA/div 4.55 ms/div	5.00 V/div 80 Hz/div

HD	Timebase 0 ms	Trigger C4 DC
12 Bits	200 ms/div 10 MS 5 MS/s	Stop 860 mA Edge Positive

4/10/2023 6:31:09 PM

Figure 4.24: SVM performance with a nonlinear load.

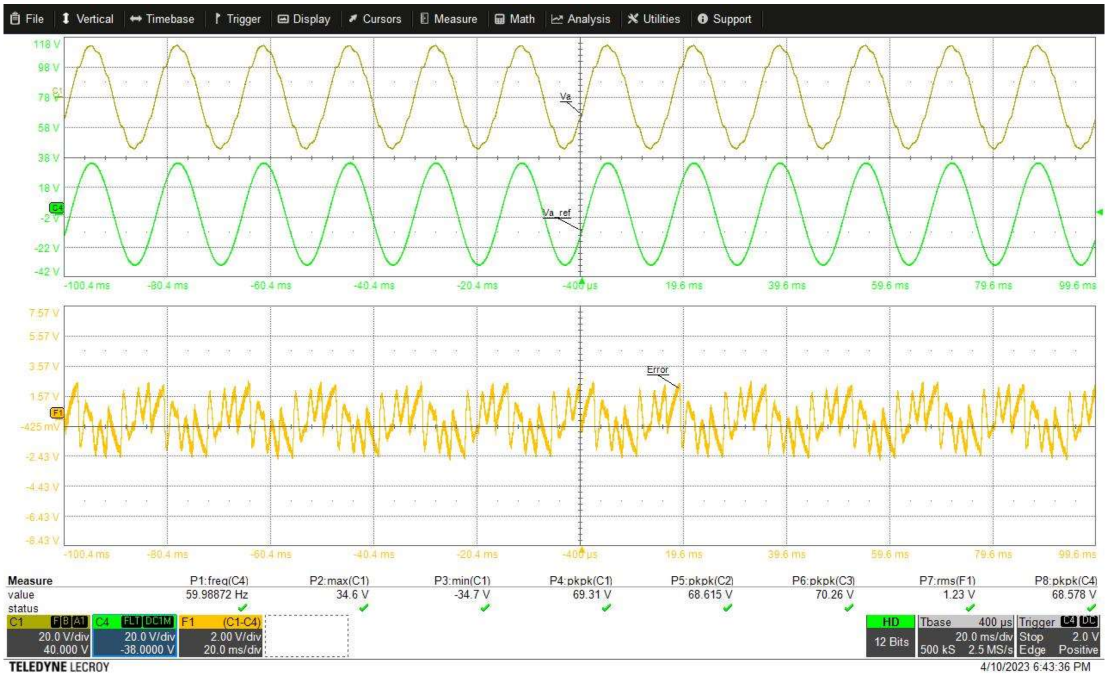

Measure	P1:freq(C4)	P2:max(C1)	P3:min(C1)	P4:pkpk(C1)	P5:pkpk(C2)	P6:pkpk(C3)	P7:rms(F1)	P8:pkpk(C4)
value	59.98872 Hz	34.6 V	-34.7 V	69.31 V	68.615 V	70.26 V	1.23 V	68.578 V
status	✓	✓	✓	✓	✓	✓	✓	✓

C1 F B A1 20.0 V/div 40.000 V
C4 FLT DC1M 20.0 V/div -38.0000 V
F1 (C1-C4) 2.00 V/div 20.0 ms/div
HD 12 Bits
Tbase 400 µs 20.0 ms/div 500 kS 2.5 MS/s
Trigger C4 DC Stop 2.0 V Edge Positive
4/10/2023 6:43:36 PM

Figure 4.25: SVM performance with a nonlinear load.

To finalize the nonlinear testing, the error and THD are compared below. As seen in previous tests, the THD for all three controllers is similar and higher than in the resistive load test as expected. None of the control models exceeded the 5% threshold assigned at the beginning of this paper. The MAE calculated showed a similar trend as with the resistive load test.

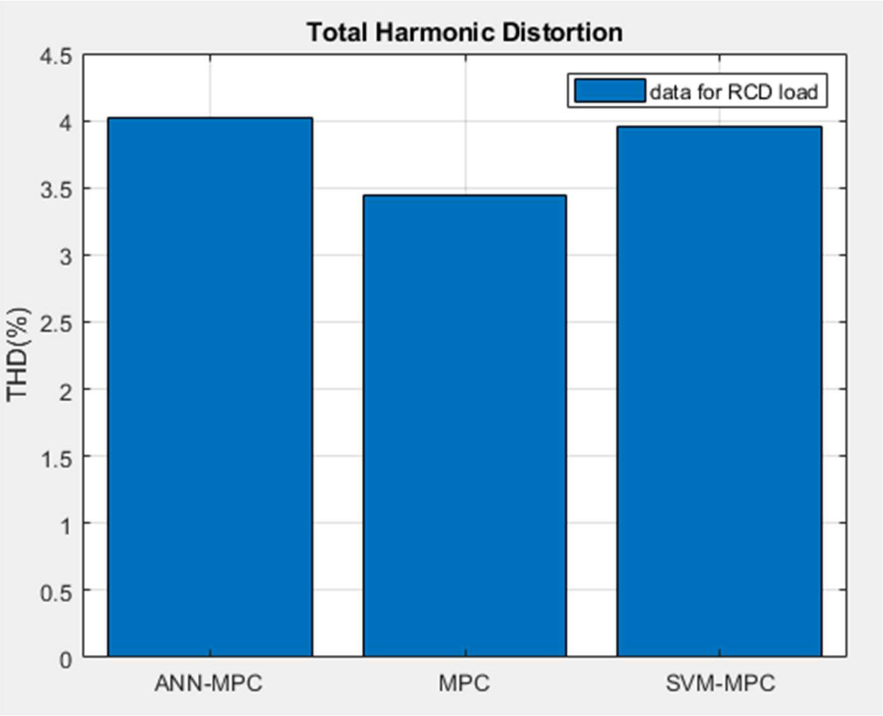

Figure 4.26: SVM performance with a nonlinear load.

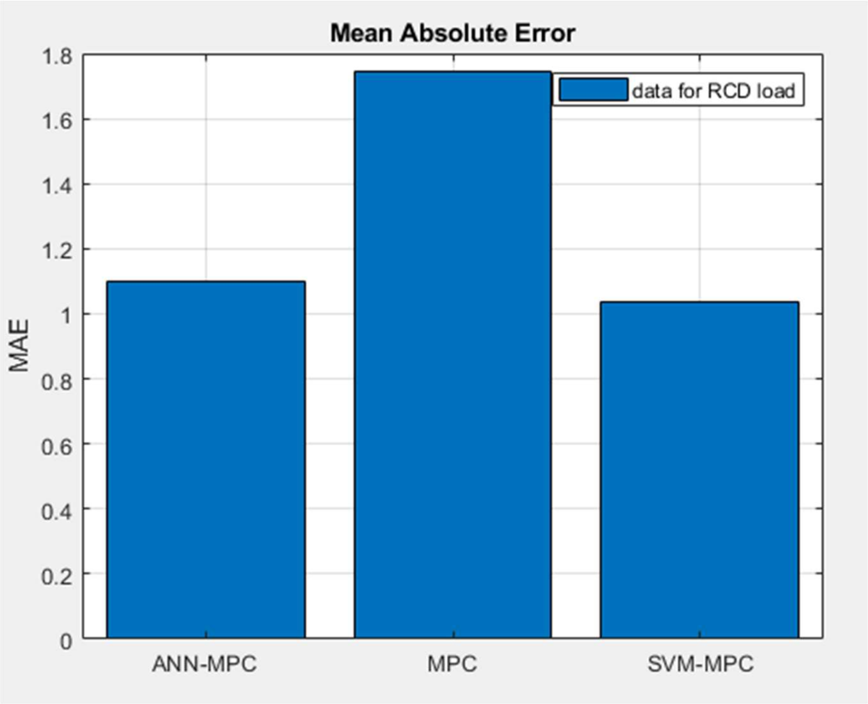

Figure 4.27: SVM performance with a nonlinear load.

4.3 Computational Time Comparison

To complete the model's comparison, a measure of the resources used by the microcontroller was taken. For this, the turnaround time maximum, mean, and standard deviation were taken. The idea was that the turnaround time would measure how long it took the microcontroller to process the data gathered during a sample period. This is done for all controller models while a static load is connected to it. Figure 4.28 shows the data collected from the MicroLabBox while the MPC model was loaded.

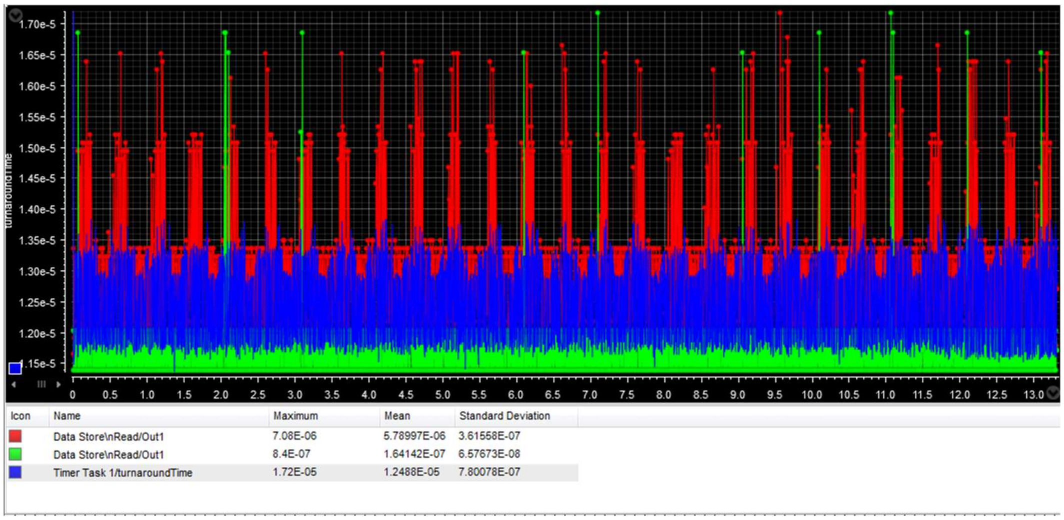

Icon	Name	Maximum	Mean	Standard Deviation
🟥	Data Store\nRead/Out1	7.08E-06	5.78997E-06	3.61558E-07
🟩	Data Store\nRead/Out1	8.4E-07	1.64142E-07	6.57673E-08
🟦	Timer Task 1/turnaroundTime	1.72E-05	1.2488E-05	7.80078E-07

Figure 4.28: Microcontroller CPU loading with MPC.

Next, the ANN-MPC was loaded in the microcontroller and the run-time data was collected as seen in figure 4.29. As implied in the previous sections in this chapter, the turnaround time is expected to be similar since there the other experimental results showed a like performance.

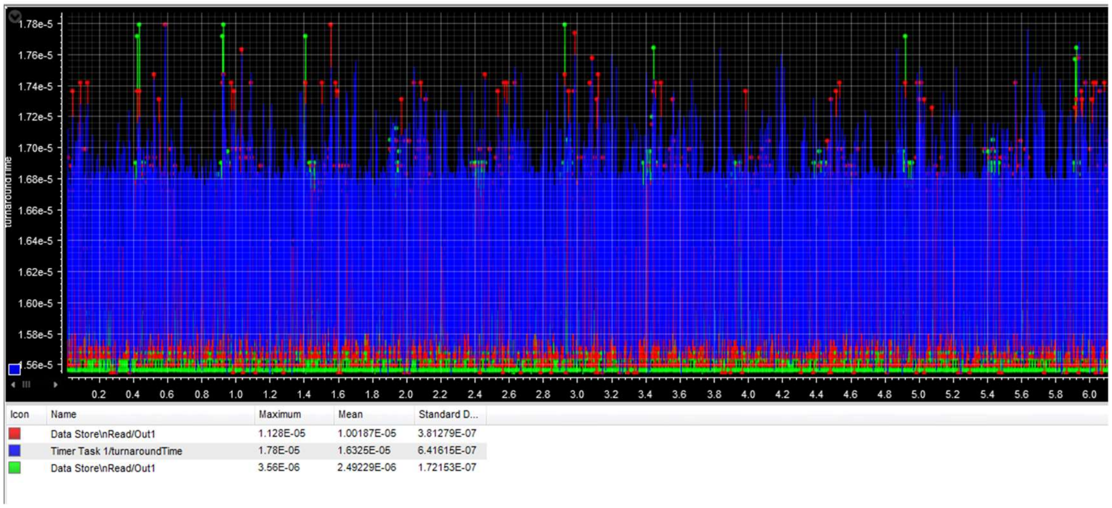

Icon	Name	Maximum	Mean	Standard D...
🟥	Data Store\nRead/Out1	1.128E-05	1.00187E-05	3.81279E-07
🟦	Timer Task 1/turnaroundTime	1.78E-05	1.6325E-05	6.41615E-07
🟩	Data Store\nRead/Out1	3.56E-06	2.49229E-06	1.72153E-07

Figure 4.29: Microcontroller CPU loading with ANN.

Finally, the data was collected for the SVM-MPC as seen in figure 4.30. Just like the ANN-MPC, the turnaround time for the SVM-MPC is within a few micro-seconds of the other two models. The maximum turnaround time for the SVM is lower than the other two control models which can explain the smaller tracking error.

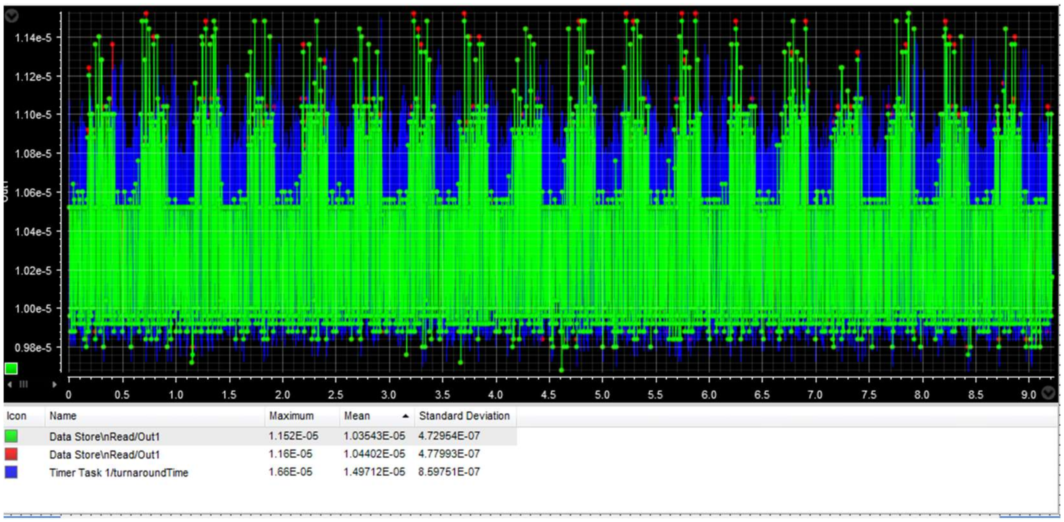

Icon	Name	Maximum	Mean ▲	Standard Deviation
🟩	Data Store\nRead/Out1	1.152E-05	1.03543E-05	4.72954E-07
🟥	Data Store\nRead/Out1	1.16E-05	1.04402E-05	4.77993E-07
🟦	Timer Task 1/turnaroundTime	1.66E-05	1.49712E-05	8.59751E-07

Figure 4.30: Microcontroller CPU loading with SVM.

Table 4.3 shows the maximum turnaround time measures for all control models. The maximum time is important because it limits the minimum sample period used. For this experimental comparison, a sample time of 20 microseconds was used. All control models had a maximum timer-task period lower than this sample time, so no problems were encountered during testing. However, the SVM-MPC did show the lowest maximum turnaround time.

	MPC	ANN-MPC	SVM-MPC
Max turnaround time (μs)	17.2	17.8	16.6

Table 4.3 turnaround time measurements.

Aside from the implied computation load similarities, these similar turnaround time measurements confirm that the ML-controls also have the fast response typically seen on the MPC.

Chapter 5 : Conclusions and Recommendations for the Future Research

The machine learning controls explored in this paper offer a viable alternative to the MPC for a three-phase inverter. The results seen chapter 4 show that the performance among the controllers is very similar and, in some cases, the MPC is exceeded by a machine learning model. The machine learning controllers also offer a simpler control model than MPC, since the MPC uses an online optimization algorithm, and the machine learning controllers are a tree of math operations. This enables the control to be easily replicated into a microcontroller that can perform these operations as demonstrated in the simulation models in chapter 3. The ML-based controllers also showed a quick response time when faced with sudden load changes which is typically seen in the MPC. In fact, the comparison showed that the ML-based control models can track the reference better than the MPC which can be attributed to the lower turnaround time observed.

These models might be able to offer an alternative to MPC applications with large prediction horizon needs for comparable performance or lower CPU resource cost. Future works might include the exploration of machine learning based controllers in other applications or modelling other controller types.

References

[1] D. L. Chandler, “Explaining the plummeting cost of solar power,” MIT News | Massachusetts Institute of Technology, https://news.mit.edu/2018/explaining-dropping-solar-cost-1120 (accessed Nov. 5, 2023).

[2] K. Hansen, “Extreme winter weather causes U.S. blackouts,” NASA Earth Observatory, https://earthobservatory.nasa.gov/images/147941/extreme-winter-weather-causes-us-blackouts (accessed Nov. 5, 2023).

[3] J. Hu, Y. Shan, K. W. Cheng, and S. Islam, “Overview of power converter control in microgrids—challenges, advances, and future trends,” *IEEE Transactions on Power Electronics*, vol. 37, no. 8, pp. 9907–9922, 2022.

[4] E. F. Camacho and C. Bordons, “Model predictive control,” *Advanced Textbooks in Control and Signal Processing*, no. 2, 2007. doi:10.1007/978-0-85729-398-5

[5] L. Zhou and M. Preindl, “Optimal tracking and resonance damping design of cascaded modular model predictive control for a common-mode stabilized grid-tied LCL inverter,” *IEEE Trans. Power Electron.*, vol. 37, no. 8, pp. 9226-9240, Aug. 2022

[6] J. Andino, P. Ayala, J. Llanos-Proaño, D. Naunay, W. Martinez, and D. Arcos-Aviles, “Constrained modulated model predictive control for a three-phase three-level voltage source inverter,” *IEEE Access*, vol. 10, pp. 10673-10687, 2022

[7] A. A. Ahmed, B. K. Koh, and Y. I. Lee, “A comparison of finite control set and continuous control set model predictive control schemes for speed control of Induction

Motors," *IEEE Transactions on Industrial Informatics*, vol. 14, no. 4, pp. 1334–1346, 2018.

[8] J. Zeng and W. Qiao, "Short-term solar power prediction using a support vector machine", *Renewable Energy*, vol. 52, pp. 118–127, 2013.

[9] C. J. C. Burges, *Data Mining and Knowledge Discovery*, vol. 2, no. 2, pp. 121–167, 1998. doi:10.1023/a:1009715923555

[10] I. Mohamed, S. Rovetta, T. Do, T. Dragicević, and A. Diab, "A neural-network-based model predictive control of three-phase inverter with an output LC filter," IEEE Access, vol. 7, pp. 124737-124749, 2019.

[11] D. Wang, Z. Shen, X, Yin, S. Tang, X. Liu, C. Zhang, J. Wang, J. Rodriguez, and M. Norambuena, "Model predictive control using artificial neural network for power converters," *IEEE Trans. Ind. Electron.*, vol. 69, no. 4, pp. 3689-3699, April 2022.

[12] S. Wang, T. Dragicevic, G. Gontijo, S. Chaudhary, and R. Teodorescu, "Machine learning emulation of model predictive control for modular multilevel converters," *IEEE Trans. Ind. Electron.*, vol. 68, no. 11, pp. 11628-11634, Nov. 2021

[13] IEEE, "*IEEE recommended practice and requirements for harmonic control in Electric Power Systems"*, Jun. 2014.

[14] A. De La Cruz, J. Zeng, T. Kim, and V. Winstead, "Comparing support vector machine and artificial neural networks based model predictive control in power converter," in *Proc. IEEE Energy Conversion Congress & Exposition*, in *Proc. IEEE Energy Convers. Congr. Exposit.*, Nashville, TN, Nov. 2023, pp. 3490-3494.

List of Publications

[1] **A. De La Cruz**, J. Zeng, T. Kim, and V. Winstead, "Comparing support vector machine and artificial neural networks based model predictive control in power converter," in *Proc. IEEE Energy Conversion Congress & Exposition*, in *Proc*. *IEEE Energy Convers. Congr. Exposit.*, Nashville, TN, Nov. 2023, pp. 3490-3494.

[2] Z. Yang, J. Zeng, and **A. De La Cruz**, "Learning and outperforming the model predictive control with a linear ϵ-support vector machine for power converter," *IEEE Trans. Ind. Electron.*, vol. 71, no. 1, pp. 5-13, Jan. 2024.